The Iceland–Faroe inflow of Atlantic water to the Nordic Seas

B. Hansen [a], S. Østerhus [b], H. Hátún [a], R. Kristiansen [a] and K. M. H. Larsen [a]

[a] Faroese Fisheries Laboratory, Box 3051, FO-110, Tórshavn, Faroe Islands
[b] Bjerknes Centre for Climate Research and Geophysical Institute, Allegaten 70, N-5007, Bergen, Norway

Abstract

The flow of Atlantic water between Iceland and the Faroe Islands is one of three current branches flowing from the Atlantic Ocean into the Nordic Seas across the Greenland–Scotland Ridge. By the heat that it carries along, it keeps the subarctic regions abnormally warm and by its import of salt, it helps maintain a high salinity and hence density in the surface waters as a precondition for thermohaline ventilation. From 1997 to 2001, a number of ADCPs have been moored on a section going north from the Faroes, crossing the inflow. Combining these measurements with decade-long CTD observations from research vessel cruises along this section, we compute the fluxes of water (volume), heat, and salt. For the period June 1997–June 2001, we found the average volume flux of Atlantic water to be 3.5±0.5 Sv (1 Sv=10^6 $m^3 \cdot s^{-1}$). When compared to recent estimates of the other branches, this implies that the Iceland–Faroe inflow is the strongest branch in terms of volume flux, transporting 47% of the total Atlantic inflow to the Arctic Mediterranean (Nordic Seas and Arctic Ocean with shelf areas). If all of the Atlantic inflow were assumed to be cooled to 0 °C, before returning to the Atlantic, the Iceland–Faroe inflow carries a heat flux of 124 ±15 TW (1 TW=10^{12} W), which is about the same as the heat carried by the inflow through the Faroe–Shetland Channel. The Iceland–Faroe Atlantic water volume flux was found to have a negligible seasonal variation and to be remarkably stable with no reversals, even on daily time scales. Out of a total of 1348 daily flux estimates, not one was directed westwards towards the Atlantic.

1. Introduction

The flow of warm, saline water from the Atlantic Ocean across the Greenland–Scotland Ridge into the Nordic Seas and the Arctic Ocean (hereafter termed "*Atlantic inflow*") is of major importance, both for the regional climate and for the global thermohaline circulation. Through its heat transport, it keeps large areas north of the Ridge much warmer, than they would otherwise have been, and free of ice. Thus, Seager et al. (2002) have computed a temperature increase due to oceanic heat transport by this flow which over large areas is considerably larger than the anticipated temperature increase during the 21st century due to anthropogenic effects. Significant reductions in the Atlantic inflow could therefore offset or even reverse the projected temperature increase in the areas most affected. At the same time, the Atlantic inflow completes the loop formed by thermohaline ventilation in the northern regions and the deep overflows back into the Atlantic across the Ridge. Thus, the salt, carried by the Atlantic inflow to the Nordic Seas, is a precondition for high densities in the upper layers and thus for the formation of intermediate and deep water. To the extent that thermohaline ventilation contributes to driving the Atlantic inflow, this opens the possibility for a positive feedback mechanism that will de-stabilize the thermohaline circulation (Broecker, Peteet, & Rind, 1985).

In spite of the obvious importance of the inflow, quantitative estimates of its fluxes of volume (mass), heat, and salt have been hard to obtain. Until recently, one of the most frequent sources for these numbers has remained that of Worthington (1970), even though he based his estimates on a few, fairly uncertain, current measurements and budgets that involved exchanges of heat and freshwater with input parameters that even today are not well known (Simonsen & Haugan, 1996). Worthington's estimate has also been questioned by later budget studies (McCartney & Talley, 1984), and quantitative estimates of the fluxes, based on

measurements, are needed to settle the uncertainties. This was a main motivation for the "Nordic WOCE" project, within which the observations reported in this paper were initiated.

The flow of Atlantic water into the Nordic Seas occurs through three main branches (Hansen & Østerhus, 2000) as shown in Fig. 1. Long-term measurements indicate that the branch west of Iceland transports slightly less than 1 Sv (10^6 $m^3 \cdot s^{-1}$) of Atlantic water (Jónsson & Briem, 2003) and therefore on the order of 10% of the total inflow. Of the other two branches, the flow through the Faroe–Shetland Channel is generally cited (explicitly or implicitly) as by far the dominant one, but there has been little evidence to support that view (Hansen, 1985).

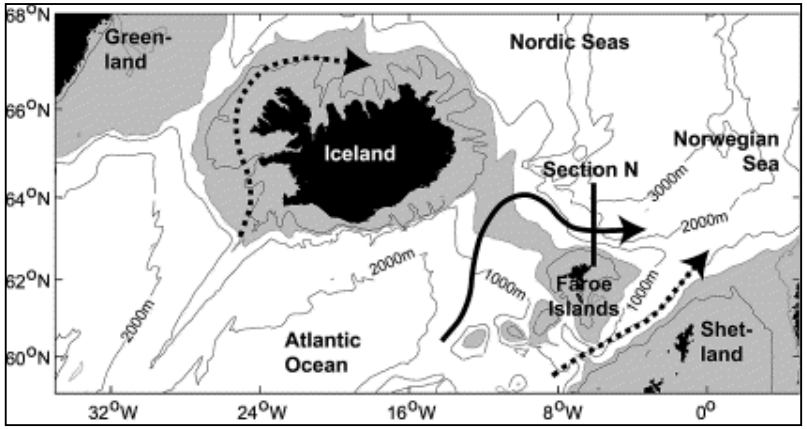

Fig. 1. The Greenland–Scotland Ridge (the shaded area on the figure indicates regions shallower than 500 m) separates the Atlantic Ocean from the Nordic Seas. Arrows indicate the three branches of Atlantic inflow to the Nordic Seas. The Faroe Current (unbroken arrow) is the branch studied in this work. The thick line termed "N" indicates the section from which most of the observations derive.

The observations, initiated in the Nordic WOCE project (Østerhus, Turrell, Hansen, Lundberg, & Buch, 2001), were therefore designed to measure fluxes through both of the gaps between Iceland and Scotland (Fig. 1). In these gaps, hydrographic (temperature and salinity) observations have been carried out on standard sections for almost a century in the Faroe–Shetland Channel and for more than a decade in the Iceland–Faroes Gap. To provide flux estimates, the Nordic WOCE project established a series of quasi-permanent mooring sites to measure currents directly. The waters surrounding the Faroes are heavily fished, and experience has taught, that traditional moorings extending far up into the water column have short survival. In the planning phase of the project, it was therefore decided to rely on the newly developed Broadband acoustic Doppler current profiler (ADCP) produced by RD Instruments. After termination of the field phase of Nordic WOCE, the measurements have continued with EU support through the two projects VEINS (Variability of Exchanges in the Northern Seas) and MAIA (Monitoring the Atlantic Inflow toward the Arctic) and from the Faroese Fisheries Laboratory (FFL). Measurements are planned to continue with support from the FP5-funded project MOEN (Meridional Overturning Exchange with the Nordic Seas) that is a component of ASOF (Arctic Subarctic Ocean Flux) study.

Here, we report on the measurements in the Iceland–Faroe Gap where the Atlantic water generally is confined to a region north of the Faroes by the Iceland–Faroes Front (Fig. 2). The measurements have mainly been carried out along a standard section (section N) crossing the Atlantic inflow branch (Fig. 2). Regular CTD surveys were initiated along this section in 1987 and, in most years since then, at least four cruises have been made. The ADCP moorings have been deployed along the same section.

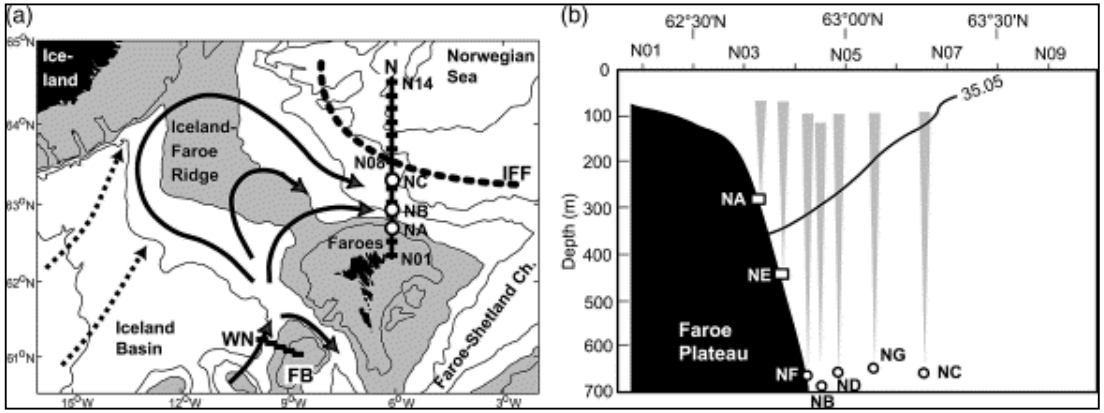

Fig. 2. Most of the observations reported in this work were collected along section N, indicated on the map (a) and shown in (b). CTD observations from five standard stations on section WN northwest from Faroe Bank (FB on a) were also used for reference. On (a), CTD standard stations are indicated by black rectangles, labeled N01–N14. Three of the ADCP mooring sites are indicated by circles labeled NA, NB, and NC. Shaded areas are shallower than 500 m. The dotted curve indicates the general location of the Iceland–Faroes Front (IFF), and arrows indicate Atlantic water pathways towards section N according to the classical view (unbroken arrows) and to alternative suggestions (broken arrows). On (b), the innermost CTD standard stations on section N are indicated as well as all the ADCP mooring sites. Rectangles indicate ADCPs in trawl-protected frames, circles indicate ADCPs in the top of moorings. Approximate ADCP ranges are indicated by gray cones. An average 35.05 isohaline (copied from Fig. 6a) indicates the typical boundary of Atlantic water on the section.

The combined CTD and ADCP data sets contain information on various oceanographical processes, including the considerable mesoscale activity which occurs in this area, but that will be treated elsewhere. In this work, we focus on the fluxes of water (mass, volume), heat, and salt through the section. Preliminary estimates of typical fluxes and their seasonal variations have previously been reported in the "grey literature", based on subsets of the data and less rigorous treatment (Hansen, Larsen, Østerhus, Turrell and Jónsson, 1999; Hansen, Østerhus, Kristiansen and Larsen, 1999 and Hansen, Jónsson, Turrell and Østerhus, 2000). These preliminary results have also been reported in two overview papers discussing the exchanges across the Greenland–Scotland Ridge (Hansen and Østerhus, 2000 and Østerhus, Turrell, Hansen, Lundberg and Buch, 2001). The objectives of this paper are threefold: (1) to document the measurements in a form more generally available to the scientific community. (2) To derive flux estimates of as high an accuracy as reasonably possible and evaluate uncertainties. (3) To evaluate variations of fluxes on time scales from a few days, through the seasonal, to the interannual.

Achieving objectives (2) and (3), requires interpolation and extrapolation of data in order to cover the whole section adequately. In addition, the Atlantic water component of the flux has to be extracted. Section N covers all the Atlantic water that has passed the Iceland–Faroe Ridge, but it also includes water that does not derive directly from the Atlantic. This is water from the East Icelandic Current and other water masses. These water masses cover variable parts of the section and, to some extent, they have already been mixed with one another before passing through the section. We use temperature and salinity characteristics to identify the Atlantic component, but to evaluate the Atlantic water flux, requires the combination of hydrographic and velocity fields, which are sampled with quite different temporal and spatial resolutions. This is a non-trivial problem, and we therefore go into considerable detail with the data processing and methods for flux calculation. This forms the main part of the paper, from 2, 3, 4 and 5 with the main results presented in 5.3 and 5.4. We end the paper with a summary of the conclusions and a discussion on the role of the Iceland–Faroe Atlantic inflow in the climate system under a global change scenario.

2. Data material

Both the hydrographic data and the current measurements were acquired on the same section, standard section N (Fig. 1), extending from 62° 20′ N 6° 05′ W to 64° 30′ N 6° 05′ W (Fig. 2). The section has depths reaching more than 3000 m, but we focus on the uppermost 600 m that contain all the Atlantic water that has passed over the Iceland–Faroe Ridge.

2.1. CTD observations

The hydrographic data were acquired during a number of cruises along standard section N in the period 1987–2001. The standard section has 14 standard stations, labeled N01–N14, with 10 nautical miles equidistant spacing between stations. Lack of time or bad weather restricted the northward extension of the section on some occasions, and a few intermediate stations have been deleted in the quality assessment procedure. Here, we only include cruises with good data from at least all the innermost 10 stations, which reduces the data set to 45 cruises. Several different CTDs of type Neil Brown, EG&G, and SeaBird have been used through the period. Since 1990, salinity samples have been obtained on each station and analyzed with an Autosal salinometer for calibration. The early CTD observations were less frequently calibrated, but the slow changes in the deep water salinities allow adjustments that keep the salinity uncertainties below 0.01. In this work, we use temperature and salinity observations averaged over 10 m depth intervals in 60 layers (bins), the uppermost one centered at 5 m depth and the deepest at 595 m.

To serve as reference for the source water characteristics of Atlantic water, we also use CTD observations from five standard stations on section WN that extends northwestwards from the Faroe Bank (Fig. 2a). These observations were treated similarly as described above.

2.2. ADCP observations

In the period October 1994–June 2001, current measurements were obtained through a number of deployments at seven different mooring sites, labeled NA, NB, … NG, along the standard section (Fig. 2b). During most of the period, instruments were deployed at the three Nordic WOCE standard mooring sites, NA, NB, and NC. From July 2000 to June 2001, the mooring at site NC was moved to site NG and two additional moorings (NE and NF) were deployed between NA and NB. At site ND, a mooring was deployed from November 1997 to June 1998. The data coverage at each of these sites is illustrated in Fig. 3, which also shows CTD cruises with full coverage of the innermost 10 stations in the same period. In the 4-year period from summer 1997 to summer 2001, there was sufficient coverage to allow volume flux estimates but, since the mooring locations changed, we split the analysis into two main periods. The first period is from summer 1997 to summer 2000 with moorings at NA, NB, and NC. The second period is from summer 2000 to summer 2001 with moorings at NA, NE, NF, NB, and NG. Table 1 summarizes details of the deployments within these two periods.

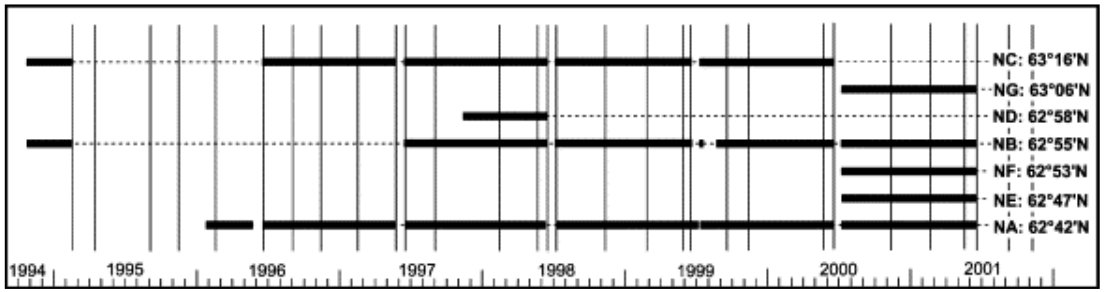

Fig. 3. Periods with successful ADCP observations at the various mooring sites (thick horizontal bars) and CTD cruises along standard section N (thin vertical lines) from October 1994 to the summer of 2001.

Table 1. Details of ADCP deployments along standard section N in the period June 1997 to June 2001. The observational period and number of days indicate whole days. The last two columns indicate the vertical extent of data for which the series of daily averaged velocities were without gaps before extrapolation and "Top" indicates the upper boundary of this range

Record	Mooring position		Depth to			Observational period		100% good	
	Latitude	Longitude	Bottom (m)	Instr (m)	Bin length (m)	yy/mm/dd–yy/mm/dd	Days	Bins	Top (m)
NA9706	62° 42.315′ N	6° 05.170′ W	300	299	10	97/06/15–98/06/08	359	1–19	103
NA9807	62° 42.178′ N	6° 05.043′ W	297	296	10	98/07/08–99/07/01	360	1–18	110
NA9907	62° 41.947′ N	6° 03.887′ W	295	294	10	99/07/03–00/06/15	349	1–17	118
NA0007	62° 42.048′ N	6° 04.456′ W	297	296	10	00/07/08–01/06/15	343	1–18	110
NE0007	62° 47.490′ N	6° 05.100′ W	456	455	25	00/07/07–01/06/15	344	1–11	147
NF0007	62° 52.700′ N	6° 05.031′ W	697	689	25	00/07/08–01/06/15	343	1–19	203
NB9706	62° 54.818′ N	6° 04.957′ W	925	659	25	97/06/14–98/06/12	365	1–18	198
NB9807	62° 55.158′ N	6° 04.844′ W	961	708	25	98/07/05–99/06/18	349	1–20	197
NB9908	62° 55.133′ N	6° 05.052′ W	957	715	25	99/08/21–00/06/15	300	1–19	229
NB0007	62° 55.106′ N	6° 05.024′ W	954	712	25	00/07/08–01/06/15	343	1–19	226
ND9711	62° 57.540′ N	6° 05.600′ W	1276	670	25	97/11/12–98/06/12	214	1–17	234
NG0007	63° 05.955′ N	6° 05.015′ W	1816	643	25	00/07/08–01/06/15	343	1–19	157
NC9706	63° 16.425′ N	6° 06.600′ W	1731	659	25	97/06/14–98/06/12	364	1–18	198
NC9807	63° 15.944′ N	6° 06.299′ W	1728	655	25	98/07/06–99/06/18	348	1–18	194
NC9907	63° 15.920′ N	6° 06.390′ W	1740	667	25	99/07/03–00/06/15	349	1–19	181

All the deployments have used upward-looking RDI ADCPs to profile the water column (Fig. 2b). At sites NA and NE, a 150 kHz RDI Broadband ADCP was placed on the bottom within a specially constructed trawl-proof protection frame (Østerhus & Hansen, 1995), with later modifications. At the other sites, 75 kHz RDI Broadband ADCPs were moored in the top of single point moorings (with the ADCP typically at depths of 600–700 m). At the deep sites, acoustic echo from the surface could be used for most of the records to infer the depth of the instrument. These observations show that drag-down of the instrument rarely exceeded 5 m and could be ignored. Sound velocity variation along the beam path was also found to be sufficiently small to be ignored.

In the early versions of the trawl-protection frame used at NA from summer 1997 to summer 1998, the steel construction affected the ADCP compass considerably. This was circumvented by two short-term calibration deployments with a traditional (Aanderaa) current meter mooring at NA while the ADCP was operating (Larsen, Hansen, Kristiansen, & Østerhus, 1999). The consistency in direction of the long-term residual flow from different deployments indicates that this procedure gave correct current direction to within a few degrees. Since summer 1998, non-magnetic aluminium frames have been used to protect the ADCPs at NA and NE. During one of the deployments at NB, one of the four ADCP sound transducers was malfunctioning. This record was therefore analyzed with only three beams, but simulations on other records at NB indicate that this has no significant effects for the averaged types of data used in this work.

The deployments at site NA were set up with a 10 m bin length (vertical averaging layer) while the other deployments had 25 m bins. Sound speed variations are sufficiently small so that the bin lengths do not need adjustment. To ensure long-term records, only one ping was used in each ensemble. This produced fairly noisy records and many observations had to be deleted during the data editing process. This process included an automatic flagging procedure, which detects outliers and large error velocities (Gordon, 1996). In addition, all observations were visually scanned in a graphical editing package, specially developed using MATLAB routines.

The resulting data sets contain a number of gaps, especially for the near-surface bins, most distant from the ADCP. In this work, high frequency variations are irrelevant and we use only daily averaged current values, but the large number of gaps in the data makes filtering difficult. Therefore, the current velocity components were de-tided before averaging. Harmonic constants were computed from the velocity data for each bin. Using these constants, the tidal signal was "predicted" for the observational period and subtracted from the original series. The Foreman FORTRAN package (Foreman, 1978) was used for both the analysis of harmonic constants and prediction. The general consistency in harmonic constants obtained from different deployments at the same site (Larsen, Hansen, Kristiansen, & Østerhus, 2000) verifies the applicability of this procedure. For each day, the de-tided velocity series were then averaged over a period as close as possible to 24 h and 50 min. Average velocity values for a bin were accepted for all days with at least 25% good coverage.

With this procedure, daily averaged current velocity components were produced for all deployments and for the deepest bins data coverage is 100% (Table 1). In the uppermost bins, the error frequency is much larger, partly due to surface reflection of side-lobes (Gordon, 1996) and partly due to range limitation. Typically, the series do, however, have more than 75% coverage up to at least the 100 m depth level.

Detailed information on moorings and data from the ADCP deployments is available in three data reports (Hansen, Larsen and Kristiansen, 1999; Larsen, Hansen and Kristiansen, 2000 and Larsen, Hansen and Kristiansen, 2001).

3. Hydrographic and velocity fields on section N

3.1. Hydrographic fields

Average sections of temperature, salinity, and density are shown in Fig. 4. Northwards from the Faroe shelf, a warm, saline area on the section identifies the wedge of Atlantic water. Its boundary towards the colder, less saline waters reaches the bottom of the Faroe Plateau at depths of 300–500 m and slopes upwards to reach the surface in the Iceland–Faroe Front between standard stations N05 and N09.

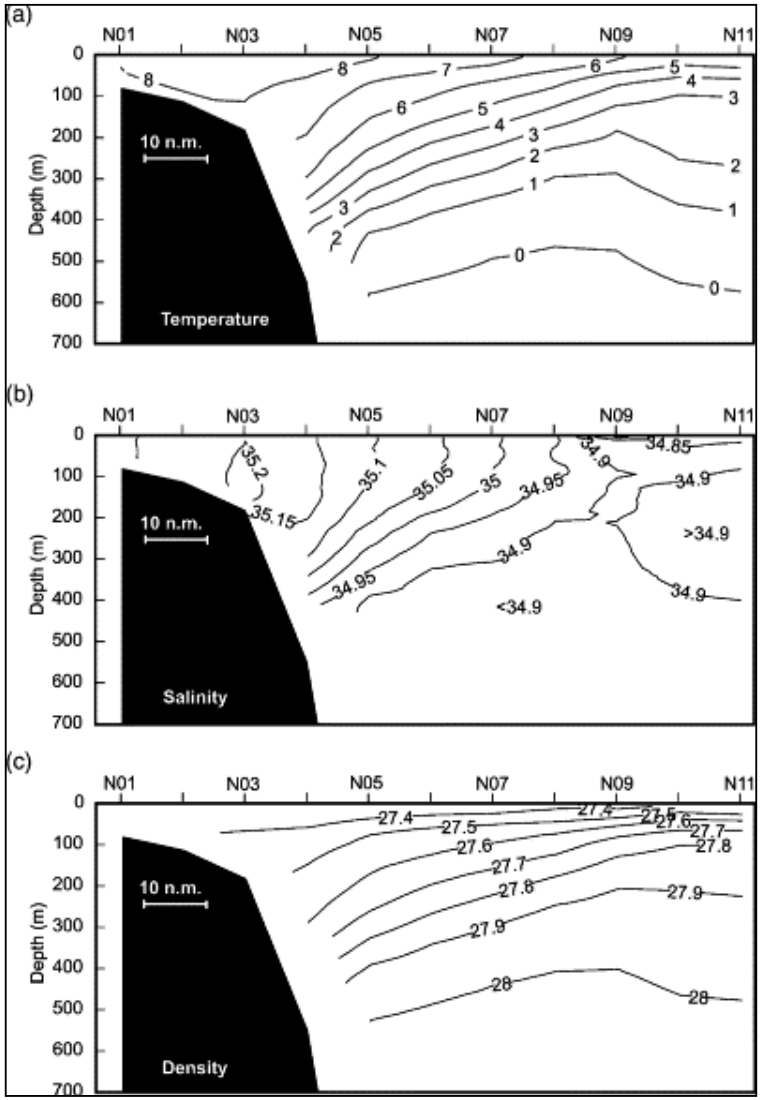

Fig. 4. Average distributions of temperature in °C (a), salinity (b), and density γ_θ in kg·m^{-3} (c) on the inner part of section N based on CTD observations by R/V Magnus Heinason in the period 1987–2001 (45 cruises for stations N01–N10, 44 cruises for station N11).

When single cruises are considered, they often look like the average distributions in Fig. 4, although usually with sharper boundaries. Meso-scale activity may deform the distribution and more irregular sections are seen occasionally (Fig. 5). When we include only cruises in the period from July 1997 to June 2001 with complete current measurements, the irregular features are smoothed out, as illustrated by the average salinity section from this period (Fig. 6a). This section looks very similar to the long-term average (Fig. 4b), although somewhat more saline. The temperature–salinity relationship on the section is illustrated in Fig. 6b, where the main water masses as described by Read and Pollard (1992) and Hansen and Østerhus (2000) are indicated.

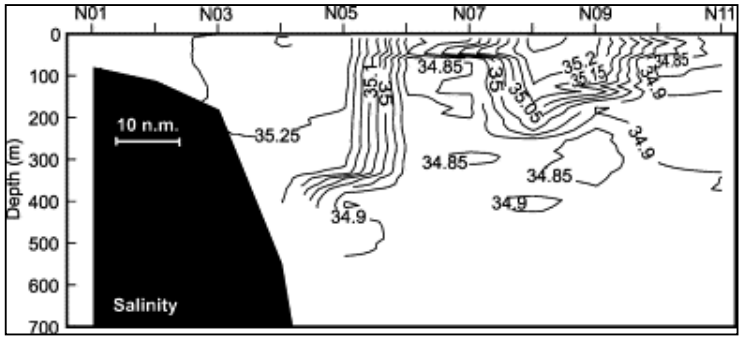

Fig. 5. Salinity distribution on standard section N, 12 June 1998.

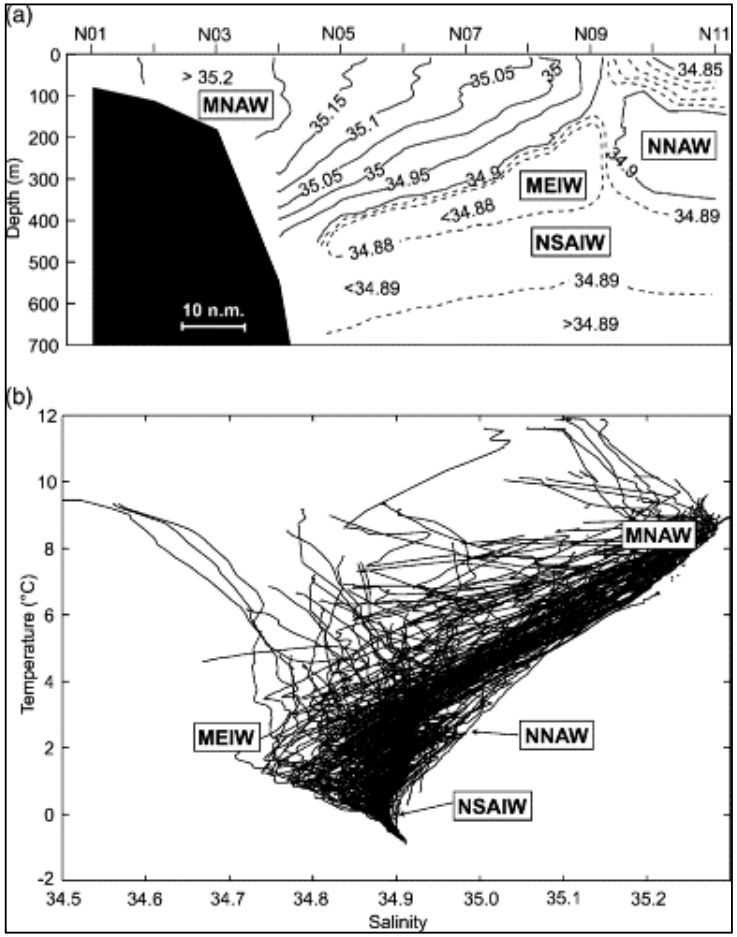

Fig. 6. Average salinity distribution (a) and TS diagram (b) for the main observational period (1997–2001). On (a), contouring interval for salinity is 0.05, except for salinities below 34.90, where broken lines indicate isohalines with contouring interval of 0.01. The main water masses are indicated.

To study the seasonal variation, the temperature and salinity fields were linearly detrended and fitted to a sinusoidal function with amplitudes and phases that were determined by a least-square algorithm for each point on the section separately. The seasonal temperature amplitude (Fig. 7a) is largest in the surface, as could be expected, but a secondary maximum is also seen at larger depths between stations N04 and N07. It seems to follow the thermocline (Fig. 4a), becoming shallower towards the north, until it surfaces in the frontal region. In the Atlantic water, above the thermocline, maximum temperatures are consistently found around August–October. The seasonal amplitude of the salinity variation (Fig. 7b) has a similar distribution as the temperature amplitude with maxima in two regions. In the surface layer, the salinity has a maximum around April–May, but the deeper amplitude maximum, close to the thermocline, culminates around August–October, as for temperature. We conclude that the areal extent of Atlantic water on the section has a seasonal variation with a maximum in autumn.

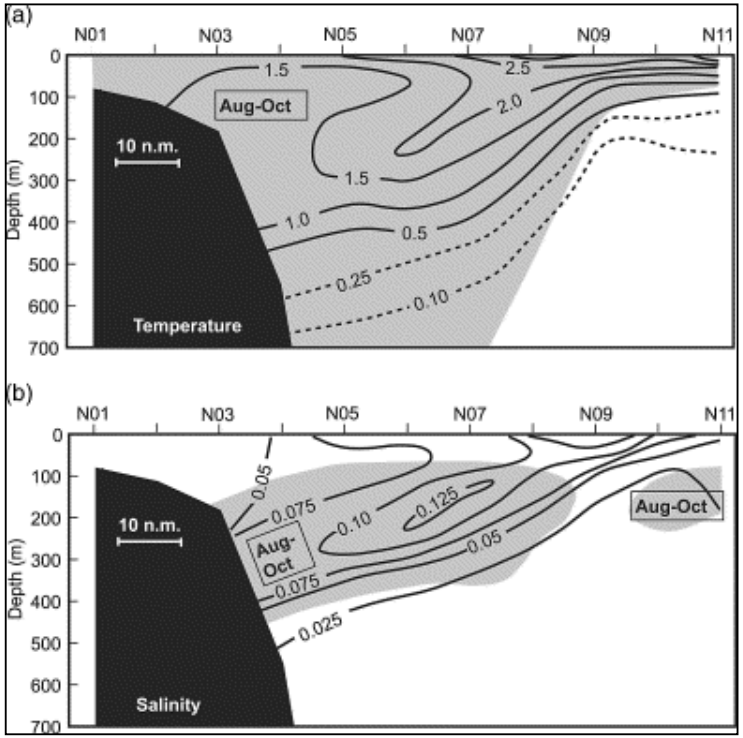

Fig. 7. Seasonal variation of temperature (a) and salinity (b) on the section. Isolines indicate magnitude of the seasonal amplitude in °C and practical salinity units, respectively. Shaded areas indicate parts of the section where maximum temperature or salinity occur in the period August–October.

In addition to the CTD observations, some information about water mass properties can be obtained from the temperature sensors in the ADCP instruments. Mostly, the instruments were located more or less constantly either in Atlantic (at site NA) or in cold water (most of the other sites) and have therefore not been very useful for indicating changes in water mass distribution. From summer 2000 to summer 2001, the ADCP at site NE was, however, located close to the typical boundary between the Atlantic and the cold waters. This is seen in Fig. 8, which shows the temperature at this site and at sites NA and NF for the same period. All these series show the temperature close to the bottom and demonstrate that the boundary moves on a wide range of time scales.

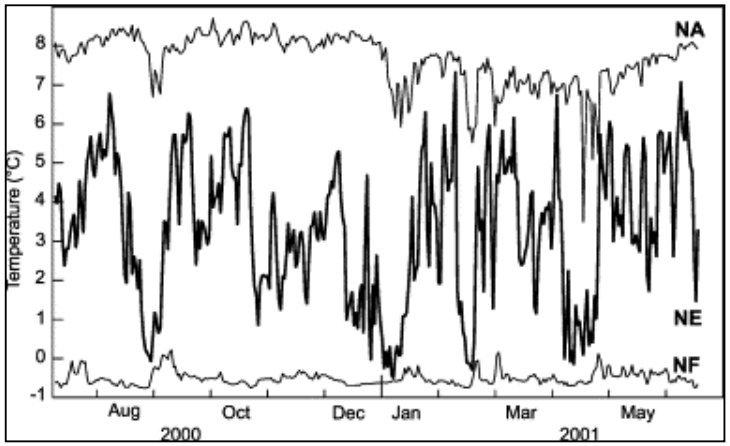

Fig. 8. Daily averaged temperature at the ADCP instruments deployed at NA, NE (thick curve), and NF from July 2000 to June 2001.

3.2. Velocity fields

The general flow through section N is illustrated by progressive vector diagrams (PVDs) in Fig. 9 with observations from one deployment at each of the sites except ND (which did not have as long a deployment period). All the records are from about 225 m depth and they show that the water at this depth has a residual flow somewhat south of east. The PVDs are all for the same duration (343 days) and their lengths therefore indicate current speed in the scale shown.

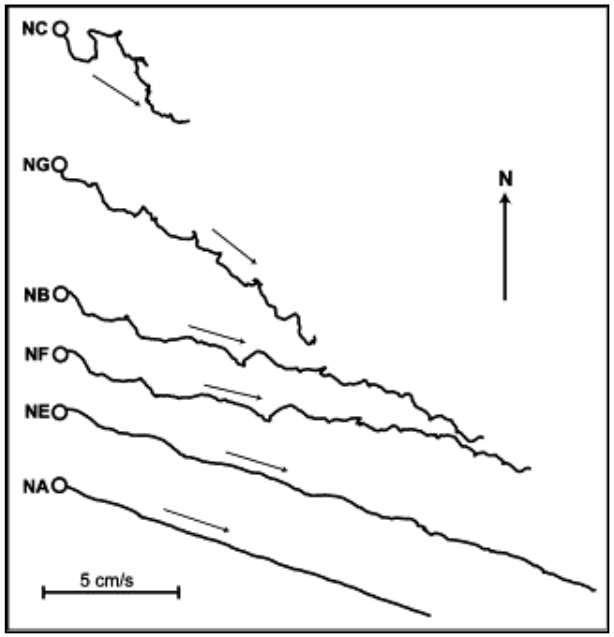

Fig. 9. PVDs for 343 days from daily averaged current at about 225 m depth for all sites with sufficient duration. At NC, a deployment from summer 1999 to summer 2000 is shown. For the other sites, the deployment was from summer 2000 to summer 2001. As all the traces have the same duration, they indicate residual flow velocity and the velocity scale is shown.

Fig. 9 indicates that the upper layer flow is to a large extent perpendicular to the section and, since this is the component responsible for the volume flux through the section, we will henceforth focus on the eastward velocity component. The vertical variation of this component (Fig. 10) has a strongly baroclinic character at the deep sites, but usually there is also flow with an eastward component below the sill depth of the Iceland–Faroe Ridge (480 m), so there is a barotropic component, as well. To illustrate the temporal variability of the flow, Fig. 11 shows the eastward component for the two sites, NA and NB, from which we have continuous time series from summer 1997 to summer 2001 except for the annual servicing periods. The flow is seen to vary on several time scales, but only occasionally is it reversed and then, only for short periods.

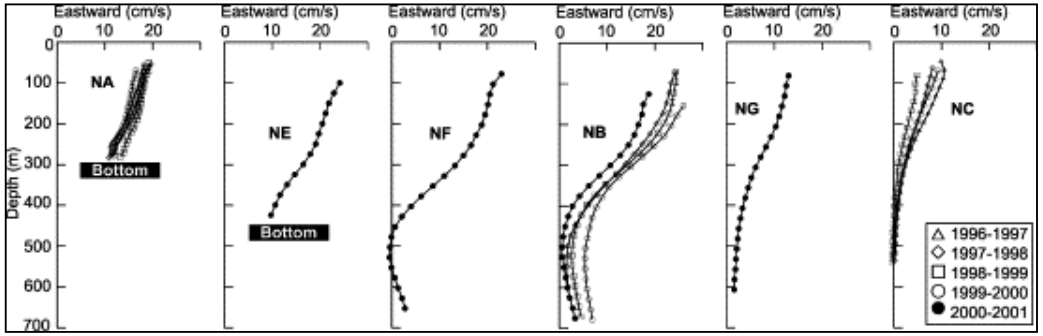

Fig. 10. Average profiles of the eastward velocities for all deployments from 1996 to 2001 with duration more than 9 months.

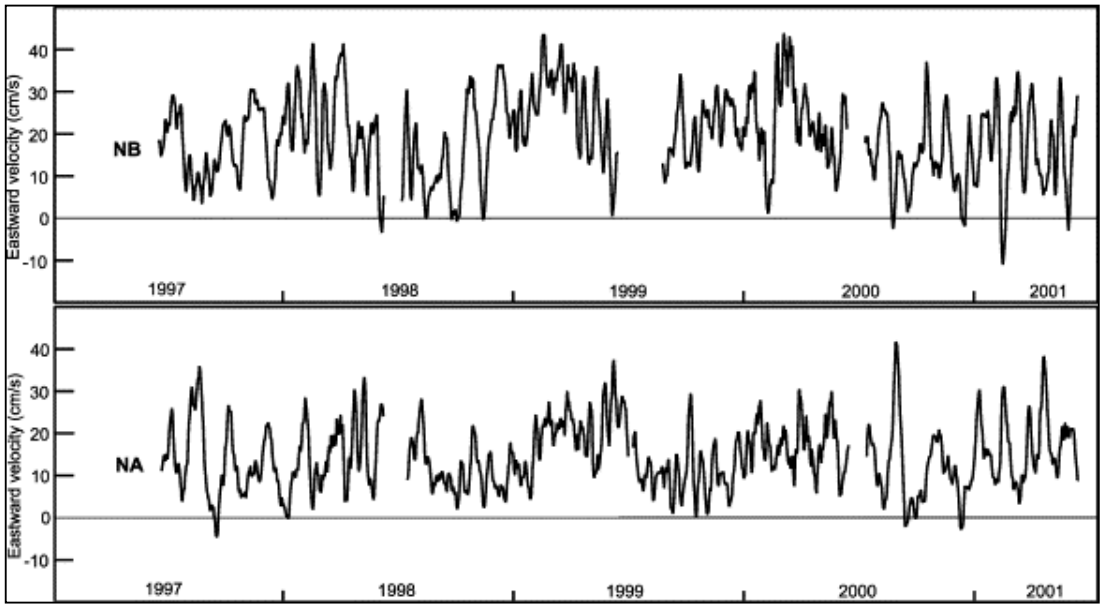

Fig. 11. Seven-day running mean of the eastward velocity component at 225 m depth from mid-June 1997 to mid-June 2001 at sites NA and NB.

The fact that the ADCP measurements do not cover the uppermost 50–100 m of the water column is a major drawback when computing volume fluxes. Including the top layer, requires vertical extrapolation, which we base on observed correlations and on geostrophy. These aspects are therefore discussed in some detail below.

3.3. Vertical velocity correlations

The relationship between velocities at different levels at the same site was investigated by correlating the eastward velocity component for pairs of bins for each deployment. An example is shown in Table 2. The numbers in the upper right triangle of the table show values for the coefficient α_{kj} that have been determined by least-square fitting to the equation:

$$u_k(t)=\alpha_{k,j}\cdot u_j(t) \quad (1)$$

for each pair of bins (k,j), where $u_k(t)$ is the eastward velocity for bin k at time t, etc. These numbers therefore are coefficients determined by a linear regression analysis with zero offset. The numbers in the lower left triangle of Table 2, similarly, are correlation coefficients between the velocities of the two bins.

Table 2. Relations between eastward velocity in different bins on the deployment at site NE from July 2000 to June 2001. Bin 1 represents the deepest layer, centered at 424 m depth while bin 15 was centered at 74 m. The lower left triangle in the table shows correlation coefficients between velocities of two different bins. The upper right triangle lists the regression coefficient in Eq. (1). From bin 1 to 11, the observations were complete with 344 days of data (Table 1). Above this level (bold types in the table), the data coverage was reduced and for bin 15, only 222 days had usable data

Bin		1	2	3	4	5	6	7	8	10	11	12	13	14	15
1		1.07	1.10	1.15	1.24	1.33	1.41	1.47	1.51	1.54	1.57	1.61	1.65	1.70	1.77
2	0.94		1.05	1.11	1.20	1.29	1.37	1.43	1.47	1.50	1.53	1.57	1.60	1.64	1.69
3	0.86	0.97		1.07	1.17	1.26	1.34	1.39	1.43	1.47	1.50	1.53	1.57	1.59	1.64
4	0.78	0.90	0.97		1.10	1.18	1.26	1.32	1.36	1.40	1.43	1.45	1.49	1.51	1.55
5	0.71	0.85	0.93	0.98		1.09	1.16	1.22	1.26	1.30	1.33	1.35	1.38	1.41	1.45
6	0.66	0.81	0.89	0.95	0.98		1.08	1.13	1.17	1.21	1.24	1.26	1.29	1.32	1.36
7	0.62	0.77	0.85	0.91	0.96	0.99		1.06	1.10	1.13	1.16	1.19	1.21	1.24	1.28
8	0.58	0.73	0.81	0.87	0.93	0.97	0.99		1.04	1.08	1.11	1.13	1.15	1.18	1.21
9	0.54	0.70	0.78	0.84	0.89	0.95	0.98	0.99		1.04	1.07	1.09	1.11	1.14	1.16
10	0.51	0.66	0.74	0.80	0.86	0.92	0.95	0.98	0.99		1.03	1.06	1.07	1.09	1.11
11	0.48	0.64	0.72	0.77	0.83	0.89	0.93	0.96	0.98	1.00		**1.02**	**1.04**	**1.05**	**1.07**
12	0.47	0.62	0.70	0.76	0.82	0.88	0.92	0.95	0.97	0.99	**1.00**		**1.02**	**1.03**	**1.05**
13	0.46	0.60	0.68	0.74	0.80	0.86	0.90	0.94	0.96	0.98	**0.99**	**0.99**		**1.01**	**1.03**
14	0.45	0.59	0.65	0.70	0.76	0.83	0.88	0.91	0.94	0.96	**0.97**	**0.98**	**0.99**		**1.02**
15	0.45	0.57	0.62	0.66	0.72	0.79	0.85	0.89	0.92	0.94	**0.95**	**0.96**	**0.97**	**0.99**	

The fact that neighbouring bins in Table 2 are well correlated, is no surprise since the instruments have a certain overlap between the bins that causes a fictitious correlation of about 15% between neighbouring bins (Gordon, 1996). The correlations in Table 2 are, however, much higher than this and extend much farther than to neighbouring bins. This implies that the temporal velocity variations have a vertically uniform character and this fact can be used to increase the data coverage of the uppermost bins. For the example in Table 2, the uppermost four bins had gaps in the time series, but using the regression coefficients in the table, the gaps can be filled with confidence as implied by the high correlation coefficients.

Using this procedure, all the deployments in the main observational period (Table 1) could be gap-filled up to depths of around 50 m for deployments at site NA and 70–100 m for the other sites. In the worst case, this involved extrapolating over seven bins. Not all the deployments had as high correlations as the example in Table 2, but the correlation coefficients were at least 0.86 for all the bin pairs used to gap-fill. In most cases, they exceeded 0.9.

After extrapolation, linear interpolation between bins was used to sub-sample the eastward velocity profile at 10 m intervals, centered at 5, 15, …, 595 m depth, whenever there was valid data. In this way, a homogeneous velocity data set with the same vertical structure as the CTD data was produced.

3.4. Geostrophy

Even after the extrapolations, discussed in the previous paragraph, there is still a surface layer, 50–100 m deep, for which we do not have velocity time series from the ADCP observations. It would, however, seem likely that the uniform character of the velocity variations, seen below this layer (Table 2), also extends into it. Unfortunately, we do not have direct velocity measurements that can be used to verify this and to estimate coefficients like the α_{kj} in Eq. (1). The hydrographic measurements do, however, extend all the way to the surface and we have therefore used the geostrophic approximation to estimate the typical vertical velocity shear in the surface layer.

The validity of the geostrophic approximation on the section as a whole is explored in Fig. 12, which compares average geostrophic velocity profiles between station pairs to average ADCP profiles from deployments between these stations. For the long-term mooring sites (NA, NB, and NC), the ADCP profiles in the figure are averages over several years. At NE, NF, and NG, the average is over about 1 year from summer 2000 to summer 2001, while the profile from ND is based on about half a year of observations. The geostrophic profiles are, on the other hand, based on 17 single CTD cruises between summer 1997 and summer 2001. When this is taken into account, the correspondence between ADCP and geostrophic profiles is remarkably good.

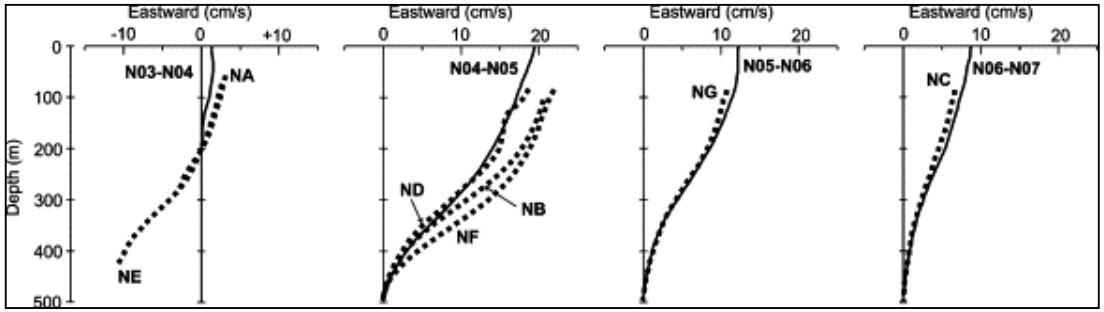

Fig. 12. Averaged eastward velocity profiles determined from geostrophy and from ADCP measurements for the uppermost 500 m. Each of the four diagrams shows the average geostrophic profile between two neighbouring standard stations (continuous curves) and average profiles for ADCPs moored between them (dashed curves). The geostrophic profiles are based on 17 cruises in the 1997–2001 period. For sites NA, NB, and NC, the ADCP profiles are the average of all records in the same period. The ADCP profiles have been offset so that they coincide with the geostrophic profiles at their deepest (reference) level.

The largest discrepancy in Fig. 12 is between station N04 and N05. This is where the current core is usually located and there is a large variation in the current both spatially and temporally which is demonstrated by the difference between the ADCP profiles in the diagram. The variability may explain part of the discrepancy, but hardly all, as indicated by Fig. 13. There, the eastward velocity difference between 200 and 500 m depth for station pair N04–N05 has been computed from 18 separate CTD cruises and compared to the velocity difference found by the ADCP at NB for the same days. There is a certain correspondence and the correlation coefficient is 0.45, which is marginally significant at the 95% level, but on the average, the geostrophic velocity differences were only 70% of the ADCP differences. We also tried to compare the geostrophic velocity differences to 3-day ADCP averages centered on the day of the cruise, but this reduced the correlation coefficient considerably.

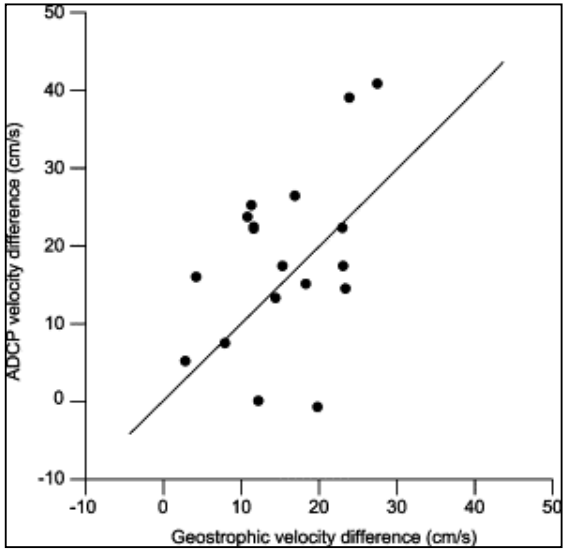

Fig. 13. Eastward velocity difference (shear) between 200 and 500 m depth measured by ADCP (daily average) at site NB compared to geostrophic shear between the same levels calculated from CTD observations at stations N04 and N05 on the same day. The line indicates equality.

In the core of the current, geostrophy thus seems to underestimate the vertical current shear somewhat, but as a whole both the sign and overall magnitude of the shear seems fairly well represented by geostrophy. This suggests the possibility of extending the ADCP measurements all the way to the surface by using geostrophy. For sites NA and NE, the geostrophic velocity profile between standard stations N03 and N04 indicates little shear and we therefore extend the ADCP measurements at these sites from the uppermost bins upwards, unchanged. The other ADCP sites have been located between standard stations N04 and N07 and there we have explored the geostrophic velocity variations by testing the two relationships:

$$u_5(t) - u_{55}(t) = \alpha \cdot (u_{105}(t) - u_{405}(t)) \quad u_{55}(t) - u_{105}(t) = \beta \cdot (u_{105}(t) - u_{405}(t)) \qquad (2)$$

where $u_5(t)$ is the eastward velocity at 5 m depth, etc. Roughly, the surface layer has been divided into two sub-layers, one from 5 to 55 m depth, and the other from 55 to 105 m depth. The vertical shear within each of these sub-layers is then related to the shear from deep water (405 m depth) to the bottom of the surface layer (105 m depth). If the geostrophic approximation is valid and if the uniform character of velocity variations extends to the surface layer, then Eqs. (2) are valid and we can estimate the coefficients α and β for each station pair.

To test this, we have correlated the geostrophic velocity differences on both sides of each of the two equations in (2), using all CTD cruises with complete coverage of the inner part of the section (Table 3). For the deeper layer (55–105 m), the correlation coefficients in Table 3 are statistically highly significant, indicating a fairly tight relationship. For the upper layer (5–55 m), the correlation coefficients are smaller, but still significant ($p<0.05$ for N06–N07 and $p<0.01$ for the other two station pairs). The table also shows the two coefficients α and β, above, determined by linear regression. For the deeper layer, the values of β are seen to be fairly similar, about 0.09, for the three station pairs considered. For the upper layer, α is more variable, but we use the value of 0.06 that applies to the two station pairs with highest correlation coefficients.

Table 3. Relations between the vertical geostrophic shear in the uppermost 100 m and the 100–400 m interval. The

vertical velocity difference across the 5–55 m and the 55–105 m depth layers, respectively, is compared to the velocity difference across the 105–405 m depth layer for each of 45 geostrophic profiles for three standard station pairs. The row termed regression factor lists the factors α (for the 5–55 m layer) and β (for the 55–105 m layer) in Eq. (2) as determined by linear regression analysis with zero offset

Station pair	Difference 5–55 m			Difference 55–105 m		
	N04–N05	N05–N06	N06–N07	N04–N05	N05–N06	N06–N07
Correlation coefficient	0.53	0.53	0.29	0.68	0.76	0.66
Regression factor	0.06	0.06	0.04	0.09	0.09	0.10

On the assumption, that the geostrophic approximation applies throughout the water column from the surface to 400 m depth (see Appendix A), Eqs. (2) can be used to extend the ADCP data all the way to the surface using the values for α and β as determined above. With these methods, all the ADCP records in Table 1 were extrapolated to cover the total depth range from the surface down to 600 m or the bottom, if shallower. Based on this, an average eastward velocity section, mainly based on the 2000–2001 period, is shown in Fig. 14.

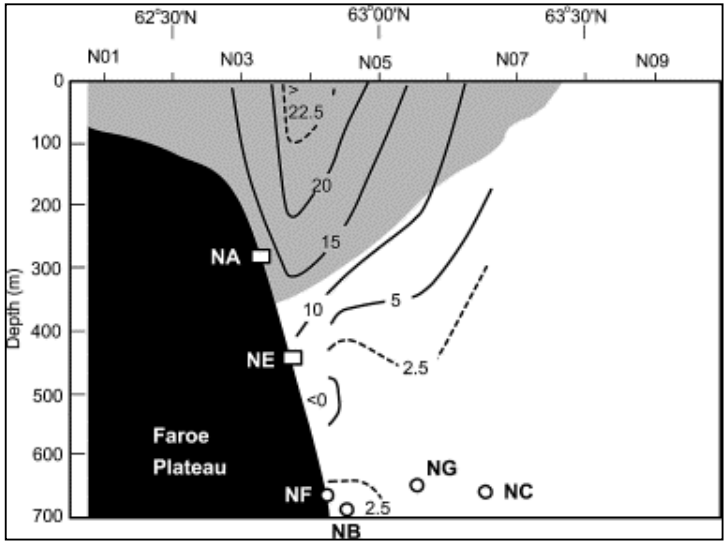

Fig. 14. The distribution of eastward velocity (in $cm \cdot s^{-1}$) on section N based on extrapolated ADCP measurements at sites NA, NE, NF, NB, and NG, using averages for the 2000–2001 period, and at site NC, using averages for the 1997–2000 period. The shaded area is on average more saline than 35.05 (Fig. 6a), representing Atlantic water.

3.5. Horizontal velocity correlations

A thorough treatment of the structure of velocity variations on the section is not within the scope of this paper (see Hátún, Hansen, & Haugan, in press). The ability of a current measuring array to cover the section adequately for flux estimation depends, however, on the distance between moorings in relation to the de-correlation distance. We therefore study the horizontal velocity correlations in the upper part of the section in Fig. 15. To this end, the average eastward velocity for the 0–200 m depth layer was calculated for each deployment and Fig. 15 shows coherence plots for pairs of mooring sites.

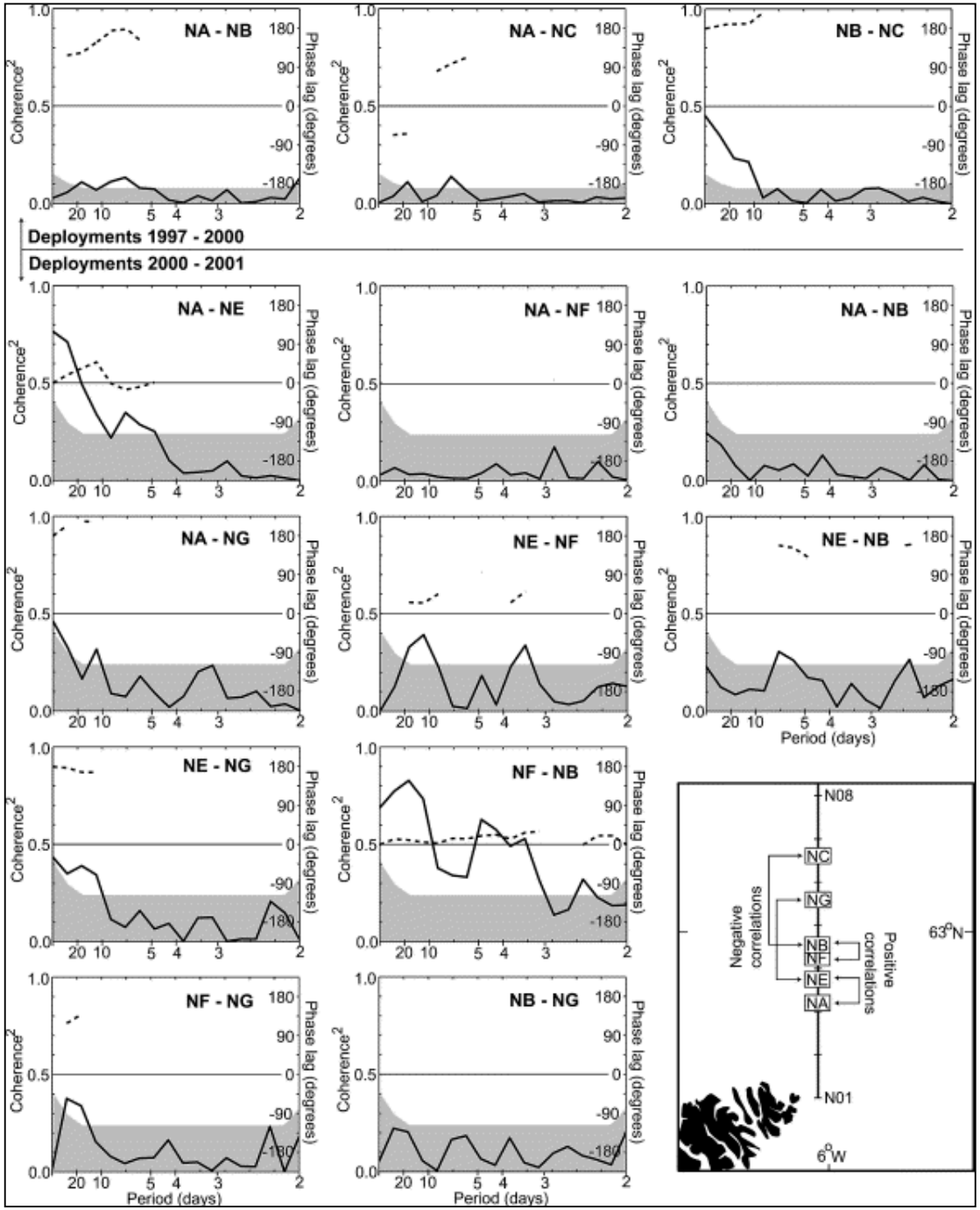

Fig. 15. Squared coherence (thick continuous curves) and phase lags (dashed curves) for pairs of eastward velocity time series (average 0–200 m) from deployments on section N. The coherence spectra were estimated using MATLAB with linear de-trending and Hanning windows with 50% overlap. In each graph, the shaded area indicates non-significance at the 99% level estimated by 10,000 Monte Carlo simulations of pairs of white noise series. Phase lag is

only shown where the squared coherence was above the 99% significance level. To facilitate interpretation, the mooring sites are illustrated in the lower right-hand corner of the graph. This panel also highlights, which pairs were strongly coherent with small phaselags (positive correlation), and which were strongly coherent with phase lags close to ±180° (negative correlation), for long-period variations.

With the exception of the pair NF–NB (and possibly NE–NF also), the coherence spectra in Fig. 15 show significant coherence only for periods of a week or longer. In this part of the spectrum, two neighbouring pairs (NA–NE and NF–NB) were strongly coherent and roughly in phase (positive correlation). Strong coherence was also found between NB and NC but with a phase lag close to 180°, indicating negative correlation at long periods. A similar, although not as strong, relationship was found between NE and NG. These negative correlations could indicate that the location of the current core moves towards and away from the shelf over long periods.

4. Total volume flux

As described above, the number and distribution of ADCP mooring sites were different in the two periods. Flux determination therefore has to be considered for each period separately and, since the second period had better instrumental coverage, we discuss that first.

4.1. Total volume flux during the 2000–2001 period

With the homogenized ADCP data set, the velocity may be integrated over the section to give estimates of total volume flux. To do this, we have divided the section into vertical columns that are 10 nautical miles wide and symmetrical around the standard stations as indicated in Fig. 16. Each column is then divided into boxes of height 10 m. The boxes are labeled by an index pair (k, j), where k varies northwards and j with depth. For each vertical column of boxes, k is given the number of the standard station in the middle of the column. In order to exclude Faroe Shelf water, the innermost column is the one centered around station N02.

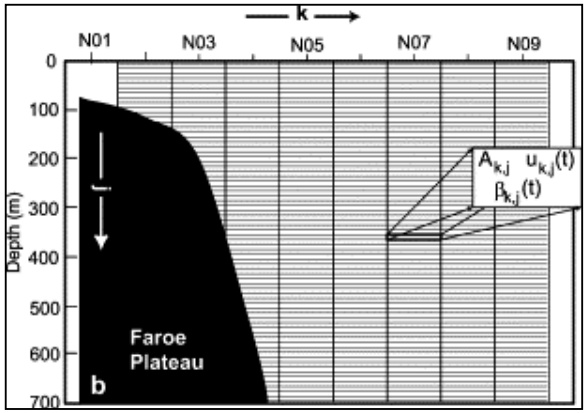

Fig. 16. Subdivision of section N into boxes for calculating fluxes. Boxes are labeled by indices k and j. One of the boxes is shown in a magnified scale indicating the parameters that must be assigned to each box: the area: $A_{k,j}$, the eastward velocity: $u_{k,j}(t)$, and the fraction of Atlantic water: $\beta_{k,j}(t)$.

With this geometry, the center of each box is at a depth where the homogenized ADCP data set has velocity values for the

different sites. We therefore linearly interpolated the velocity between the mooring sites and prescribed constant values outside the mooring array, and then piece-wise averaged the resulting velocity distributions to obtain eastward velocity values $u_{k,j}(t)$ for the boxes of Fig. 16. For the area south of the moorings, we have used measurements with traditional

Aanderaa current meters, which indicate typical residual velocities on the order of 6 cm s^{-1} in the vicinity of N02 (Hansen & Larsen, 1999), as indicated in Fig. 17. Similarly, we have used the average velocity profile at NC, based on the ADCP measurements in the 1997–2000 period to extend the velocity northwards from NG. As indicated in Fig. 17, we have even extended it north of site NC. This was motivated by the average geostrophic profiles between the three station pairs N06–N07, N07–N08, and N08–N09. All of these indicated a similar eastward velocity difference around 7–9 cm s^{-1} between 500 m depth and the surface. Deep boxes that intersect the bottom or are close to the slope may not have any ADCP velocity on the inner side, because the inner ADCPs are at shallower sites. For these boxes, we use the same interpolation method assuming a fictitious velocity below the inner ADCPs equal to the velocity at the deepest bin (see Appendix A).

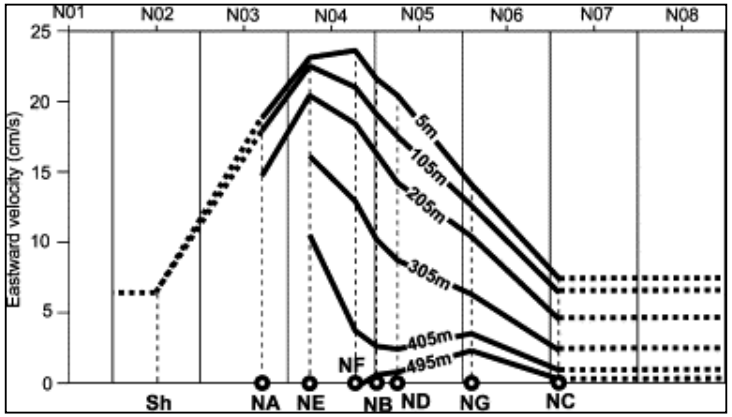

Fig. 17. The latitudinal variation of the average eastward velocity on section N for six different depths (thick continuous lines) based on averaged ADCP profiles. For sites NA, NE, NF, NB, and NG, the 2000–2001 period is used. The values for NC are based on the 1997–2000 period while the values for ND are for the deployment there, but scaled with the NB values to adjust for temporal variation. (As an example, the surface value at ND was reduced by 18%, because the surface velocity at NB was this much weaker during the ND deployment than in the 2000–2001 period.) The thick dashed lines extend the average velocity variation for flux calculations as described in the text. The continuous vertical lines, midway between standard stations, define the vertical columns that the section is divided into for flux calculations.

In this way, the average eastward velocity for each box can be derived from the ADCP measurements for every day in the deployment period and the total volume flux of water each day, $V_T(t)$, is then:

$$V_T(t) = \sum_k \sum_j A_{k,j} \cdot u_{k,j}(t) \qquad (3)$$

where $A_{k,j}$ is the area of the box at depth number j for standard station number k, equal to 1.852×10^5 m^2 for boxes that do not intersect the bottom and equal to zero for boxes, totally below the bottom. In Fig. 18, it is seen how the average volume flux varies as the northern limit of integration is extended out to station N08, which normally covers all the Atlantic water (Fig. 6). Most of the flux passes through the columns

under standard stations N04 and N05.

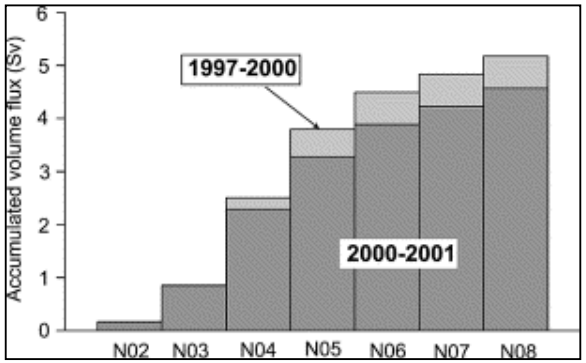

Fig. 18. Accumulated total volume flux from station N02 northwards, from the surface to 600 m depth. Columns with dark shading show the average for the 2000–2001 period while the lighter shading is for the 1997–2000 period.

4.2. Total volume flux during the 1997–2000 period

In the first measurement period, only sites NA, NB, and NC were occupied and in the preliminary estimate, reported by Hansen, Østerhus et al. (1999), the velocity between the ADCPs was assumed to vary linearly between NA and NB. The 2000–2001 measurements clearly show that this was not a good approximation (Fig. 17), but they also indicate a fairly high correlation between the velocities in the intermediate waters and at the two sites, at least for periods of a week or more (Fig. 15).

This opens the possibility that the velocities between NA and NB can be expressed by the velocities at these two sites. We have tested the models:

$$u_{\mathrm{NE},j}(t) = \gamma_{\mathrm{NE},j} \cdot u_{\mathrm{NA},j}(t) + \lambda_{\mathrm{NE},j} \cdot u_{\mathrm{NB},j}(t) \quad u_{\mathrm{NF},j}(t) = \gamma_{\mathrm{NF},j} \cdot u_{\mathrm{NA},j}(t) + \lambda_{\mathrm{NF},j} \cdot u_{\mathrm{NB},j}(t) \qquad (4)$$

where $u_{\mathrm{NE},j}(t)$ is the eastward velocity at depth j for site NE at time t, etc. The factors γ and λ were determined for each depth level by multiple linear regression analysis of the data from the 2000–2001 period. We have also tested models with one of the velocity series from NA or NB, only. However, both $u_{\mathrm{NE},j}(t)$ and $u_{\mathrm{NF},j}(t)$ are better described by the multiple regression models in Eqs. (4), even at depths below the ADCP at NA (300 m). When the regression coefficients are determined for all depths, j, Eqs. (4) can be used to determine interpolated velocities between NA and NB, which allows calculation of the volume flux without using data from NE and NF.

The accuracy of this method was tested by comparing volume fluxes through the inner part of the section for the 2000–2001 period, calculated in this way with the fluxes using the measurements from NE and NF (Fig. 19). For daily flux estimates, the correlation coefficient was 0.985 and with weekly averages, it increased to 0.994. The average flux over the whole period (343 days) was 1% smaller when using Eqs. (4) rather than the measured values. We also tested a multiple regression model with offsets included in

Eqs. (4). The 1% discrepancy in average flux disappeared, but the correlation did not increase. Since we see no physical reason for an offset, we choose not to add more degrees of freedom to the model and used Eqs. (4) without offsets.

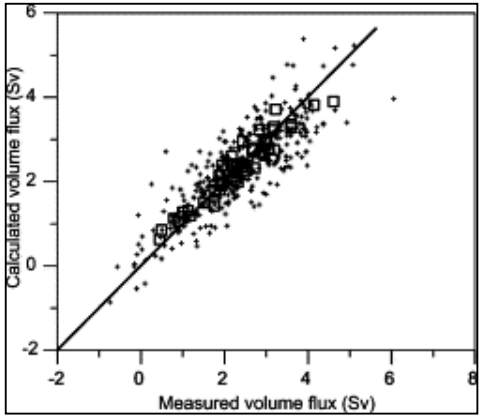

Fig. 19. The volume flux through the columns under N02, N03, and N04 during the 2000–2001 period, determined by using Eqs. (4) instead of the measured velocities at NE and NF (calculated volume flux) compared to the flux determined by using all the measured ADCP data (measured volume flux). Pluses indicate daily average flux. Open squares indicate 7-day averages. The line indicates equality.

The high correlation coefficient and the close relationship in Fig. 19 indicate that Eqs. (4) are a good approximation and we have therefore used these relationships with the regression coefficients determined from the 2000–2001 period to calculate the flux in the 1997–2000 period when NE and NF were not occupied. In this period, NG was not occupied either, but NC was. We do not have simultaneous measurements at NB, NG, and NC and can therefore not do a multiple regression analysis as for NE and NF. We could use the 2000–2001 measurements to regress NG on NB only, but the low correlation between these two sites (Fig. 15) argues against that. Instead, we simply assume that the velocity in the 1997–2000 period varies linearly from NB to NC. As indicated in Fig. 17, this seems to be a good approximation in the average, and presumably on long time scales for the water at 300 m depth, and above. At deeper layers, this does not seem to be a good approximation, but very little Atlantic water is found there so, the flux estimate of Atlantic water will not be much affected by this.

Using this method, the volume flux of water above the 600 m level from N02 to N08 was calculated for the 1997–2000 period. As shown in Fig. 18, the average flux was found to be higher in this period than in the 2000–2001 period. Whether this difference is statistically significant is, however, doubtful, when error sources (Appendix A) and variability are considered. Averaged over the whole period, the total volume flux through this part of the section was estimated to 5.0 Sv with variations, which on monthly means ranged between 1.8 and 8.7 Sv (Fig. 20).

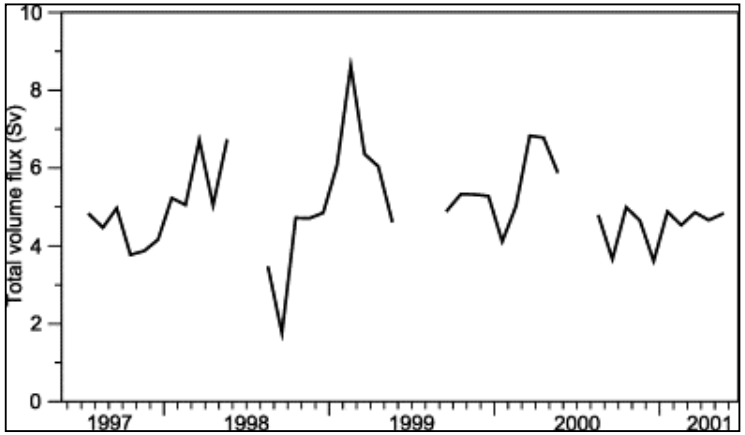

Fig. 20. Monthly averaged total volume flux through section N from 62°25′ N to 63°35′ N and from the surface down to 600 m. Only months with complete coverage were included.

5. Flux of Atlantic water

The total volume flux (Fig. 19), computed from Eq. (3), includes all the Atlantic water that passes through section N but, in addition, it also includes water that has not crossed the Iceland–Faroe Ridge recently (Fig. 6). Eq. (3) can, however, be modified by introducing a parameter, β, defined as the fraction of Atlantic water. If $\beta_{k,j}(t)$ is the Atlantic water fraction for the box (k, j) at time t (Fig. 16), the Atlantic water flux, $V_A(t)$, will be given by:

$$V_A(t) = \sum_k \sum_j \beta_{k,j}(t) \cdot A_{k,j} \cdot u_{k,j}(t) \quad (5)$$

With $A_{k,j}$ and $u_{k,j}(t)$ determined as previously described, calculation of Atlantic water flux is, thus, reduced to estimation of $\beta_{k,j}(t)$ for each box as a function of time. Several methods have in the past been used for this purpose in similar cases, usually based on relating in situ temperature and/or salinity characteristics to assumed source values for the water masses involved. Determination of the Atlantic water fraction, $\beta_{k,j}(t)$, therefore involves two different problems, determination of in situ water characteristics on section N, and determination of source water characteristics.

5.1. Generating daily fields for in situ temperature and salinity on section N

In order to use temperature and salinity to determine $\beta_{k,j}(t)$ in Eq. (5), we need the values of these parameters at every point of the section and for every day from June 1997 to June 2001, except for the annual ADCP servicing periods. Measured values are only available for the few days in this period when a CTD cruise took place and there is no reason to believe that interpolation between these dates would

give realistic values. Including the established seasonal variation (Fig. 7) may help, but, in addition, daily temperature and salinity values on the section can, to some extent, be derived from the velocity field observed with the ADCPs. This should come as no surprise, since these fields are connected through geostrophy, and the inverse method, deriving velocity from temperature and salinity, was the backbone of classical oceanography.

As with the classical dynamical method, there are problems in deriving temperature and salinity from velocity, but Hátún et al. (in press) have shown that the problems, to a large extent, can be overcome by using empirical orthogonal function (EOF) analysis. This technique uses statistical methods on observed data to separate the spatial and the temporal variations so that, e.g. the temperature $T_{k,j}(t)$ in box (k, j) can be expressed as:

$$T_{k,j}(t) = T_{k,j}^{avg} + t \cdot T_{k,j}^{tr} + T_{k,j}^{ampl} \cdot \cos\left(\frac{2\pi}{365} \cdot t - T_{k,j}^{phase}\right) + PC\_T1(t) \cdot EOF\_T1_{k,j} + PC\_T2(t) \cdot EOF\_T2_{k,j} + \cdots \quad (6)$$

Here, t is the day number since January 1, 1997, $T_{k,j}^{avg}$ and $T_{k,j}^{tr}$ represent the average temperature field and a linear trend field, respectively. $T_{k,j}^{ampl}$ and $T_{k,j}^{phase}$ represent amplitude and phase of the seasonal variation at each point (k, j) of the section and were presented in Fig. 7a. In addition to these terms, Eq. (6) includes a number of terms containing EOF modes ($EOF\_T1_{k,j}$, etc.) with spatial variation, which are modulated by their associated principal components ($PC\_T1(t)$, …) that vary with time. In principle, a large number of modes are needed on the right-hand side of Eq. (6) to get exact equality, but for the temperature and salinity fields on section N, Hátún et al. (in press) found that most of the variance was explained by the first EOF modes. They furthermore found that the principal components for these modes were highly correlated to one of the principal components of the velocity field. This means that to a large extent the temperature (and salinity) field can be reconstructed from the ADCP velocity data:

$$T_{k,j}(t) = T_{k,j}^{avg} + t \cdot T_{k,j}^{tr} + T_{k,j}^{ampl} \cdot \cos\left(\frac{2\pi}{365} \cdot t - T_{k,j}^{phase}\right) + a_T \cdot PC\_C(t) \cdot EOF\_T1_{k,j} \quad (7)$$

where $PC\_C(t)$ is the principal component for the velocity mode that is well correlated to the principal component of the dominant temperature EOF mode and a_T is a conversion factor between the current and temperature variations. Using the data presented in our study, Hátún et al. (in press) evaluated all the terms on the right-hand side of Eq. (7) and its salinity equivalent.

The "reconstructed" temperature field, based on Eq. (7), explained 60% of the total observed temperature variance on the section and the "reconstructed" salinity field explained 44% of the total salinity variance. Hátún et al. (in press) also compared the observed temperature at the bottom of site NE (Fig. 8) to the "reconstructed" temperature at this location. Site NE is not in the area where the EOF has its largest variation. Nevertheless, the correlation coefficient between the measured and the "reconstructed" series was found to be 0.75, based on de-seasoned daily values. This independent check confirms that the temperature field, reconstructed by Eq. (7), does indeed explain a substantial part of the observed temperature variations. We have therefore used Eq. (7) and its salinity equivalent to determine daily values for $\beta_{k,j}(t)$ in Eq. (5).

From Eq. (7) and its salinity equivalent, we can evaluate the temperature and salinity distribution of the water carried through the section. For each day in the 1997–2001 period, the boxes in Fig. 16 are sorted into temperature classes of width 0.5 °C and salinity classes of width 0.025. Average volume fluxes for each class are then computed from Eq. (3). The results from this are shown by the bar charts in Fig. 21. The figure also shows accumulated volume fluxes. As could be expected, Eq. (7) generates a high variability, which extends the range of both temperature and salinity variations beyond what is found in nature, but with small flux contributions and, over most of the range, we expect Fig. 21 to be relatively accurate. Both the temperature and the salinity flux

distribution have maxima that are characteristic for Atlantic water (slightly above 7 °C and around 35.2). This illustrates the dominance of Atlantic water in the flux through the section, but we note also the presence of other water masses, especially by the secondary salinity maximum, just below 34.90, which indicates Norwegian Sea Arctic intermediate water (NSAIW) (Fig. 6b).

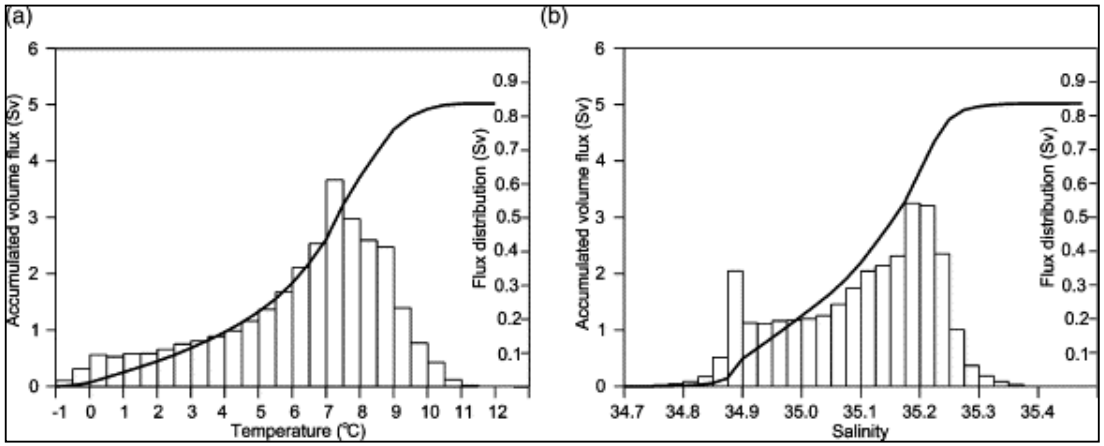

Fig. 21. Volume flux of water through section N from 62°25′ N to 63°35′ N and from the surface down to 600 m subdivided into temperature (a) and salinity (b) classes. In each panel, the bar chart shows the flux within each temperature or salinity class, scaled by the vertical axis on the right-hand side of the panel. The continuous curves show the accumulated flux, obtained by summing the values in the classes, scaled by the vertical axis on the left-hand side of each panel.

5.2. Source water characteristics

The in situ characteristics on section N arise through mixing between various source water masses, modified by air–sea interaction. Since we focus on fluxes across the Iceland–Faroe Ridge, the Atlantic source water is by definition the water in the upper layers (down to about 500 m) due west of the Ridge. This water is often termed modified North Atlantic water (MNAW, Fig. 6). Due to winter convection, this water mass is generally fairly homogeneous in the vertical, but it varies considerably in the horizontal. It is therefore important to consider from what areas the Atlantic water flow over the Iceland–Faroe Ridge is drawn. In the classical description (Fig. 39 in Helland-Hansen & Nansen, 1909), all the water is drawn from a branch of the North Atlantic Current located north of Faroe Bank. Section WN on Fig. 2a crosses this current and Fig. 22 shows average temperature and salinity on that section in the period 1998–2001.

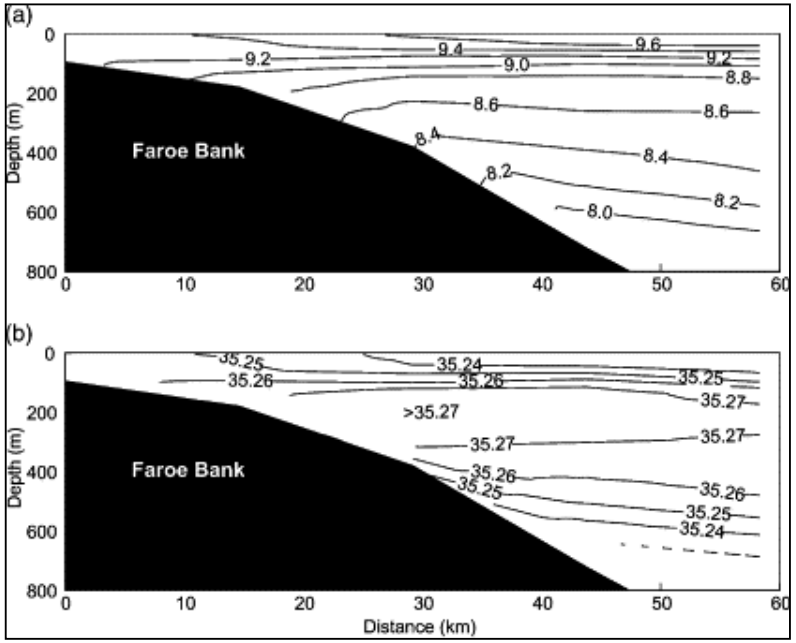

Fig. 22. Average temperature (a) and salinity (b) on section WN (Fig. 2a) based on eight CTD cruises between 1998 and 2001.

Comparing the characteristics on section WN (Fig. 22) to those on section N (Fig. 4 and Fig. 6), both temperature and salinity are seen to be slightly lower on section N. Since the Atlantic water is more saline than all other water masses on section N, the Atlantic core on that section may be defined as a maximum salinity layer. The de-seasoned characteristics of this core (Fig. 23) varied considerably during the last decade, but remained fairly constant in the 1997–2001 period (Fig. 23). On the average, the Atlantic core on section N is found to be 0.02–0.04 fresher and 0.25–0.5 °C colder than the water on section WN (Fig. 22). To some extent, this may be due to air–sea interaction during the passage from section WN to section N. Hansen and Østerhus (2000) estimated annual decreases of 0.02 in salinity and 1 °C in temperature for Atlantic water in this region. They also cited observations of drifters that required more than half a year to cross the Ridge. Other drifters were, however, observed to cross much faster and it is not likely that air–sea interaction is the sole cause of the difference between section WN (Fig. 22) and the Atlantic core on section N (Fig. 23).

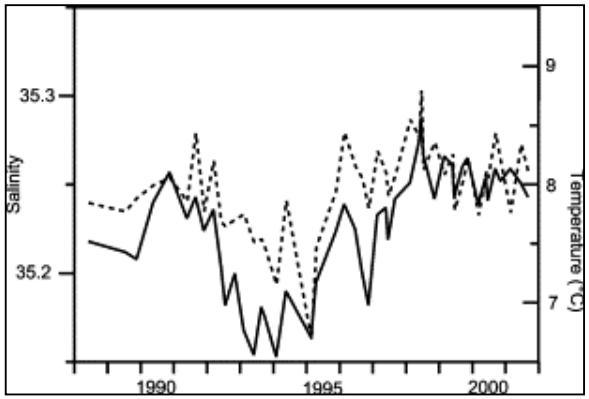

Fig. 23. Temperature (dashed line) and salinity (full line) of the core of Atlantic water on section N determined from CTD surveys. The core is defined as that level of 50 m vertical extension on the section that has the highest average salinity. The curves have been "de-seasoned" by subtracting a sinusoidal variation, determined by least-square fitting.

If it is assumed that all Atlantic water on section N must have passed through or close to section WN (continuous arrows in Fig. 2a), this difference implies that even the Atlantic core on section N has been admixed by fresher and colder non-Atlantic waters. There is, however, evidence that some of the Atlantic water, at least, takes a different path. Based on satellite tracked drifter observations, Valdimarsson and Malmberg (1999) suggested an alternative path with the Atlantic water flowing closer to Iceland on its way towards the ridge (broken arrows in Fig. 2a) and Orvik and Niiler (2002) suggest that this is the main path. Water brought along this path would be considerably fresher and colder than on section WN.

With contribution from different branches with different characteristics, a single set of temperature and salinity values for the source characteristics of Atlantic water on section N requires a volumetric averaging over the different contributions. At the present state of knowledge, this cannot be done in a meaningful way. The temperature and salinity values in Fig. 22 may be considered to represent maximum values, but representative source values may be considerably lower. To allow for this uncertainty, we have done several calculations with temperatures ranging between 7 and 9 °C and salinities between 35.20 and 35.27 for the source characteristics of the Atlantic water mass, which we denote as MNAW (Table 4).

Table 4. Average volume, heat, and salt flux, as well as average temperature and salinity of Atlantic water through section N for the period June 1997 to June 2001 with different assumptions about mixing model and source water characteristics of MNAW and MEIW. To the characteristics of MNAW shown in the table was added a seasonal variation with an amplitude of 0.58 °C for temperature and 0.02 for salinity and with a maximum in September for both parameters. The unit for heat flux is TW (10^{12} W) and for salt flux, it is kT·s^{-1} (10^{6} kg·s^{-1})

Mixing model	MNAW source		MEIW source		Volume flux (Sv)	Heat flux (TW)	Salt flux (kT s^{-1})	Average	
	Temperature (°C)	Salinity	Temperature (°C)	Salinity				Temperature (°C)	Salinity
3-Point	8.00	35.23	2.00	34.75	3.54	124	128	8.17	35.23
3-Point	9.00	35.27	2.00	34.75	3.17	123	115	9.00	35.27
3-Point	7.00	35.20	2.00	34.75	3.81	125	138	7.67	35.20
3-Point	8.00	35.23	1.00	34.70	3.68	130	134	8.20	35.22
3-Point	8.00	35.23	3.00	34.70	3.50	123	126	8.15	35.23
3-Point	8.00	35.23	1.00	34.80	3.63	128	131	8.19	35.22
3-Point	8.00	35.23	3.00	34.80	3.37	117	122	8.11	35.23
s-Ref	Reference SALINITY=35.10				2.86	96	104	7.80	35.19
s-Ref	Reference SALINITY=35.05				3.40	111	123	7.58	35.17
s-Ref	Reference SALINITY=35.00				3.81	120	138	7.35	35.15
t-Ref	Reference temperature (°C)=7.00				2.57	90	92	8.13	35.19
t-Ref	Reference temperature (°C)=6.00				3.30	110	119	7.74	35.17
t-Ref	Reference temperature (°C)=5.00				3.78	121	137	7.44	35.15

In addition to the MNAW, a number of other source waters occur on section N (Fig. 6), but only NSAIW and modified East Icelandic water (MEIW) get into contact with the Atlantic source water over extended areas. The NSAIW has fairly well defined characteristics (T=0.5 °C, S=34.9) both in the literature (Hansen & Østerhus, 2000) and in Fig. 6. The MEIW has much more variable characteristics (Hansen & Østerhus, 2000) and, to a large extent, it seems to be formed in the region (Read & Pollard, 1992) with contribution of MNAW. As source water, we should use the other components from which MEIW is formed. These seem to enter in variable mixing ratios but all of them are considerably fresher than both the MNAW and the NSAIW. We therefore use temperatures ranging between 1 and 3 °C and salinities between 34.7 and 34.8 for the source characteristics of MEIW (Table 4).

5.3. Average fluxes of Atlantic water, heat, and salt

With information on in situ and source water characteristics, various methods can be used to determine the Atlantic water fraction $\beta_{k,j}(t)$. A common practice in the Nordic Seas is to define a reference salinity and assign the value, β=1, to all boxes with salinity above the reference, while the value, β=0, is assigned to the rest of the boxes. Table 4 shows average Atlantic water flux calculated with this method (mixing model: *s*-ref) and with three different choices for reference salinity. Similarly, one can define a reference temperature and Table 4 lists average fluxes with three different choices of reference temperature (mixing model: *t*-ref).

Another method can be used if only three, well defined, water masses are involved and modification by air–sea interaction can be ignored. If typical temperatures and salinities of these three source water masses are known, a simple 3-point mixing model (Hermann, 1967) allows the determination of the relative content of MNAW water from the temperature and salinity at each point. The

Atlantic water fraction $\beta_{k,j}(t)$ for each box on the section can then be calculated from the temperature and salinity characteristics of the box. As mentioned above, MNAW mixes mainly with MEIW and NSAIW. In Table 4, we have therefore calculated average Atlantic water flux with this mixing model and with different combinations of source water characteristics for MNAW and MEIW.

It has been noted that the in situ temperature and salinity on section N vary seasonally (Fig. 7) and this is taken into account in Eq. (7) and the equivalent salinity equation. In a similar manner, seasonal variations of source water characteristics must be considered. For MNAW, the observations of the Atlantic core on section N show a seasonal variation with an amplitude of 0.58 °C for temperature and 0.02 for salinity and with a maximum in September for both parameters. These values might seem to be too small when compared with Fig. 7, but this is because the location of the core, defined as the salinity maximum, varies during the season. This seasonal variation of MNAW source water was taken when calculating the fluxes in Table 4. For NSAIW, the source water characteristics are fairly stable without appreciable seasonal variation, while for MEIW, we have too little information to estimate seasonal variation. For these two water masses, the characteristics were therefore assumed not to vary seasonally.

In addition to volume fluxes, Table 4 also lists average fluxes of heat and salt through the section. By definition, the heat flux depends on the amount of heat lost within the system, rather than the temperature, as such. Most of the water flowing out of the Arctic Mediterranean has temperatures close to 0 °C and we therefore compute the heat flux by multiplying each term in Eq. (5) by temperature, heat capacity, and density. In contrast to temperature, the salinity differs significantly from one outflow branch to another. We therefore compute the salt flux by multiplying each term in Eq. (5) by salinity and density. To the extent that salinity represents salt concentration (within 0.5%), this results in an "absolute" salt flux. Some of the heat and salt carried through the section derives from other sources than the Atlantic and care has to be taken when only the fluxes that have come directly across the Iceland–Faroe Ridge are to be calculated. When other water masses than MNAW are present in a box ($\beta_{k,j}<1$), in situ temperature and salinity are not equal to the values for the Atlantic water. In these cases, the assumed source characteristics of MNAW were used for temperature and salinity rather than in situ values.

The last two columns in Table 4 show average temperature and salinity for the Atlantic water flowing through the section. Average temperature was defined as the heat flux divided by the Atlantic water flux, heat capacity, and density, while average salinity was defined as the salt flux divided by the Atlantic water flux and density. These values clearly depend on the assumptions made about water mass characteristics, but with a smaller range of variation.

From the examination of error sources (Appendix A), it appears that their effects on the average Atlantic water flux are small compared to the uncertainty introduced by uncertain source water characteristics as seen in Table 4. From that table, it is clear that the somewhat arbitrary choice of a reference salinity or a reference temperature affects the result considerably. We therefore prefer the 3-point mixing model. Combining the results from the upper part of Table 4 with the error estimates discussed, we conclude that the average Atlantic water flux for the 1997–2001 period was 3.5 ±0.5 Sv. Similarly, the heat and salt carried by the Atlantic water was found to be 124±15 TW (referenced to 0 °C) and $(128\pm15)\times10^6$ kg·s^{-1}, respectively. These estimates are quite similar to the preliminary estimates, based on a less thorough treatment of the ADCP measurements from 1997 to 1999 (Hansen, Østerhus et al., 1999).

5.4. Flux variations

Fluxes of water, heat, and salt will vary due to velocity variations as well as variations in the Atlantic water fraction. In order to study flux variations, the source water characteristics and mixing model have to be chosen and, in the following, we use the values in the top line of Table 4 with seasonal variation for MNAW source values, as discussed. With this choice, Atlantic water flux can be estimated for each of the 1348 days with sufficient ADCP coverage in the combined summer 1997 to summer 2001 period (Fig. 24). The daily estimates, as well as weekly averaged values, show variability on several time scales.

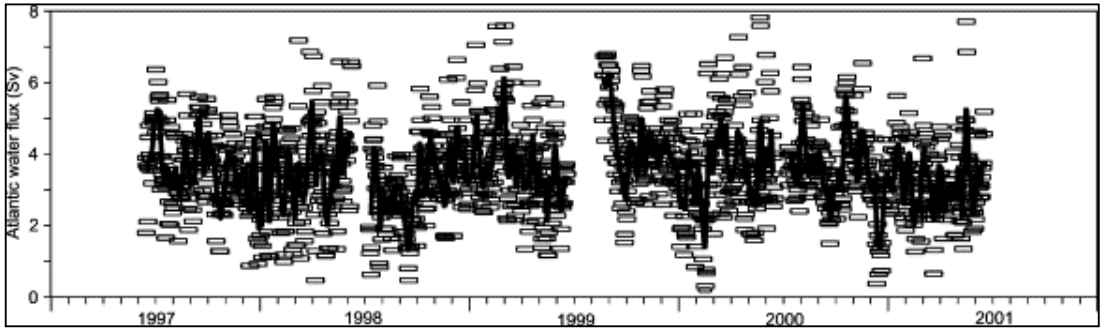

Fig. 24. Volume flux of Atlantic water through section N from June 1997 to June 2001. Rectangles indicate daily values. Continuous lines indicate 7-day running average values.

Seasonal variation of various parameters was studied by fitting time series of eastward velocity at a key point of the section, total volume flux, Atlantic water flux, heat flux, and salt flux to a sinusoidal seasonal model in a least-squares manner (Table 5). The total volume flux showed a consistent seasonal variation with an amplitude slightly less than 20% of the average flux and with a maximum in March–April, but the Atlantic water flux does not have a pronounced seasonal variation (Fig. 25). The reason for this is that both the velocity field (total volume flux) and the areal extent of Atlantic water on the section (Fig. 7) vary seasonally, but with almost opposite phases. The heat flux carried by the Atlantic water has its maximum in late summer, as could be expected, but the salt flux carried by the Atlantic water does not have an appreciable seasonal amplitude.

Table 5. Results of fitting various parameters to a sinusoidal seasonal model. Numbers in brackets for amplitude indicate percentage magnitude of amplitude relative to average value. Max-day is the day number in the year when the model predicts maximum to occur. Total volume flux is through that part of section N, which is from 62°25′ N to 63°35′ N and from the surface down to 600 m

Parameter	Average	Amplitude	Max-day
East vel. at 195 m at NB (cm s^{-1})	20.4	5.4 (26%)	47
Total volume flux (Sv)	5.01	0.88 (18%)	90
Atlantic water flux (Sv)	3.55	0.08 (2%)	242
Heat flux (TW)	125	15 (12%)	245
Salt flux (10^6 kg·s^{-1})	128	3 (2%)	241

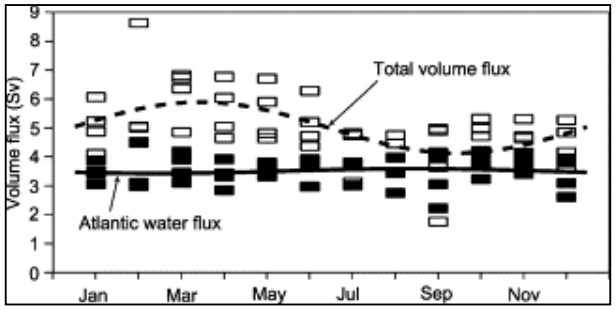

Fig. 25. Seasonal variation of the total volume flux (open rectangles) and Atlantic water flux (filled rectangles) through section N. Each rectangle indicates monthly average for 1 month with at least 15 days of observations. Curves show seasonal variation determined by model fit (Table 5) of total volume flux (dashed curve) and Atlantic water flux (continuous curve).

In the preliminary report by Hansen et al. (2000), it was concluded that "if there is a consistent seasonal variation in the inflow of Atlantic water between Iceland and the Faroes, then it is probably relatively small, with an amplitude on the order of 0.5–1 Sv with a minimum in July–August". The results from the present study (Table 5) are not in conflict with this, but they narrow the range of a possible seasonal variation considerably. The negligible seasonal amplitude of the Atlantic water flux is somewhat dependent on the method used. If we had assumed constant temperature and

salinity fields, we would have found a significant seasonal amplitude (0.64 Sv), in phase with the volume flux. This is, however, in conflict with the observed seasonal variation of these fields (Fig. 7). The results in Table 5 are also based on the assumed seasonal amplitudes for the source characteristics of MNAW (0.58 °C and 0.02), but we tried to multiply these amplitudes by a factor of three, which only increased the seasonal amplitude of the Atlantic water flux to 0.25 Sv in a sinusoidal model fit. Thus, a seasonal amplitude for the Iceland–Faroe Atlantic water flux below 10% of the average value would seem to be a robust result.

In their latest estimate, Turrell, Hansen, Hughes, and Østerhus (2003) find the Faroe–Shetland Channel net inflow to have a small seasonal amplitude (0.2 Sv), with maximum in autumn. The inflow west of Iceland is much weaker (slightly less than 1 Sv) (Jónsson & Briem, 2003) than the other two branches in terms of average fluxes, but Stefánsson (1962) reported an appreciable seasonal variation of this branch with maximum in summer.

These results may be compared to the measurements by Orvik, Skagseth, and Mork (2001) who found that the Atlantic water flux through the Svinøy section, farther east in the Norwegian Sea, had a pronounced seasonal variation. The Atlantic water flows through the Svinøy section as a broad current with two branches that are fed both by the Iceland–Faroe inflow and the inflow through the Faroe–Shetland Channel. For the eastern branch, the seasonal variation found by Orvik et al. (2001) is compatible with our results and those of Turrell et al. (2003), if we assume that a larger fraction of the Iceland–Faroe inflow is steered into the eastern Svinøy section branch in winter. Such a variation has been observed in the Faroe–Shetland Channel by Turrell et al. (2003). This explanation implies that the western Svinøy section branch should be weaker in winter, in contrast to the findings by Orvik et al. (2001). Their results for the western branch were, however, inferred from hydrography and include therefore only the baroclinic part of the flow.

Interannual variation was studied by averaging Atlantic water flux and other parameters over the same period for each of the four deployments. The result (Table 6) shows some interannual variation, especially between the 1999–2000 and the 2000–2001 deployment periods. However, the Atlantic water flux only varies by about 16% between these two periods. With only 4 years of observations, any conclusions as to long-term trends in fluxes would be premature.

Table 6. Interannual variation. Average values of various parameters, averaged over the same period (22 August–8 June) for the four deployment periods. Total volume flux is through that part of section N, which is from 62°25′ N to 63°35′ N and from the surface down to 600 m

Parameter	1997–1998	1998–1999	1999–2000	2000–2001
East vel. at 195 m at NB (cm s^{-1})	21.0	23.8	23.7	15.8
Total volume flux (Sv)	5.18	5.22	5.55	4.53
Atlantic water flux (Sv)	3.50	3.53	3.86	3.30
Heat flux (TW)	121	121	135	115
Salt flux (10^6 kg·s^{-1})	126	128	140	119

The variability on shorter time scales can be illustrated by a power spectrum of the Atlantic water flux (Fig. 26), which indicates that there is little variance on time scales of a few days. Fifty-three percent of the power in Fig. 26 was found at periods of 10 days or more. There seems to be an indication of a peak in the spectrum for periods around a week, but the reality and possible cause of this feature remain an object for future work. It should also be stressed that much of the variability on short time scales may be fictitious and derive from limited coverage of the section.

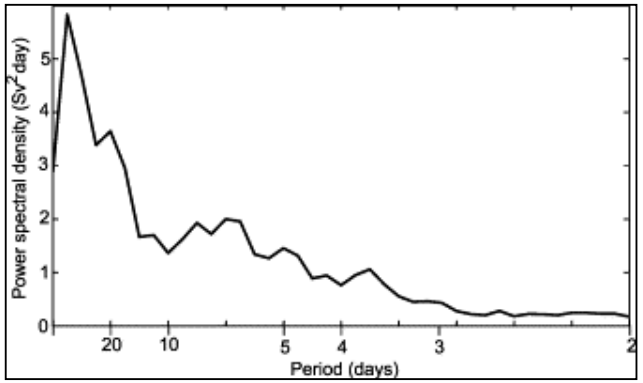

Fig. 26. Power spectrum of the Atlantic water flux for the period from summer 1997 to summer 2001, as an average of four spectra, each from one deployment.

A notable feature of the short-term flux variability is demonstrated by Fig. 24. At a first glance, the daily flux values in this figure might give the impression of large variability. Note, however, that none of the 1348 daily flux estimates were negative, implying westward flow towards the Atlantic. This is in contrast to the velocity records from individual sites. The current velocity at specific locations may well show occasional reversal, even when averaged over a week (Fig. 11). When integrated over the section to produce flux values, these reversals are, however, canceled out. The values in Fig. 24 are, of course, not an exact representation of the actual Atlantic water flux for each day. Instrumental inaccuracies, limited coverage, and the approximations, which we have made, introduce errors in the flux estimate. These effects would, however, be expected to increase, rather than decrease, variability in the flux estimates. Thus, the actual Atlantic water flux should be less variable and even less likely to reverse, than indicated in Fig. 24. Even on daily time scales, the Iceland–Faroe Atlantic inflow is, thus, a highly stable flow.

6. Conclusions and outlook

The results obtained in this work confirm that the Iceland–Faroe branch of the Atlantic inflow is an important component in the budget of the Arctic Mediterranean. With an average flux of 3.5±0.5 Sv, it carries slightly more Atlantic water than the branch that flows through the Faroe–Shetland Channel (3.2 Sv), according to the latest estimate (Turrell et al., 2003), and several times more than the Atlantic water flux of the branch west of Iceland (around 0.8 Sv according to Jónsson & Briem, 2003, and S. Jónsson, personal communication, 2003). With these estimates, the Iceland–Faroe branch carries 47% of the total Atlantic inflow to the Arctic Mediterranean and 42% of the total oceanic inflow, when the Pacific water flow through the Bering Strait is included (Roach et al., 1995).

To determine the importance of the Iceland–Faroe inflow branch in the heat and salt (freshwater) budgets of the Arctic Mediterranean, all of the exchange branches and their connections have to be considered. This is beyond the scope of this paper but, if we maintain the approximation that all of the outflows are close to zero in temperature, then the heat transport of the Iceland–Faroe inflow will be 124±15 TW. This is of the same magnitude as the heat flux carried by the Faroe–Shetland inflow (123 TW), according to Turrell et al. (2003). The average salt flux carried by the Iceland–Faroe inflow was estimated to $(128\pm15)\times10^6$ kg·s^{-1}, which is slightly above the salt flux through the Faroe–Shetland Channel (115×10^6 kg·s^{-1}), according to Turrell et al. (2003).

The Iceland–Faroe Atlantic inflow branch to the Nordic Seas, thus plays an important role in maintaining the volume, heat, and salt balances of the Arctic Mediterranean, and it is appropriate to consider how this role may be affected by anthropogenically induced climate change. Hansen and Østerhus (2000) have argued that the Atlantic inflow to the Nordic Seas is mainly driven by thermohaline forcing. Several (Rahmstorf, 1999), although not all (Latif, 2001), climate models predict a reduced thermohaline circulation as a consequence of anthropogenic carbon dioxide emission and Hansen, Turrell, and Østerhus (2001) have found observational evidence for reduced Iceland–Scotland overflow during the last half of the 20th century. If this decrease has not been compensated by increases in other overflow branches, the total inflow must have been decreased as well. Since the Iceland–Faroe branch seems to be the dominant inflow branch, a decrease in the volume flux of this inflow seems probable.

The observations, reported here, are of too short duration to allow any conclusions as to trends. Altimeter records indicate that the sea-surface slope from Iceland to the Faroes was slightly decreasing in the period 1993–2000 (D. Quadfasel, personal communication, 2003) and this might indicate a concurrent reduction in Iceland–Faroe Atlantic inflow, but more direct evidence is clearly needed. A continued monitoring of the inflow with moored equipment therefore has a high priority and the observational system must have an accuracy that can allow detection of relatively small changes. The system described in this work seems to have this capability and continued operation is planned. With support from the 5th Framework Programme of Europe, continuation has been secured until summer 2005. With successful operation, this will extend the time series to a length of 8 years, which may be sufficient to identify trends, if they are pronounced and persistent.

Acknowledgements

The observations reported in this work have received funding from the "Environmental Research Programme of the Nordic Council of Ministers (NMR) 1993–1998", from the Danish and Norwegian Research Councils (Nordic WOCE project), from EU-MAST4 (VEINS project), and from the Fifth Framework Programme of the European Commission (MAIA project). This is publication no. A37 of the Bjerknes Centre for Climate Research.

References

Broecker, W.S., Peteet, D.M. and Rind, O., 1985. Does the ocean–atmosphere system have more than one stable mode of operation?. *Nature* **315**, pp. 21–26.

Foreman, M. (1978). *Manual for tidal currents analysis and prediction*. Pacific Marine Science Report, 78-6.

Gordon, L., 1996. Acoustic Doppler current profiler. Principles of operation. In: *A practical primer* (2nd ed.), RD Instruments, p. 55.

Hansen, B., 1985. The circulation of the northern part of the Northeast Atlantic. *Rit Fiskideildar* **9**, pp. 110–126.

Hansen, B., & Larsen, K. M. H. (1999). *Traditional current meter observations in Faroese offshore waters 1977–1994. Data Report*. Technical Report, The Faroese Fisheries Laboratory, 99–01, 193 p.

Hansen, B., Larsen, K. M. H., & Kristiansen, R. (1999). *ADCP deployments in Faroese waters 1997–1999*. Technical Report, The Faroese Fisheries Laboratory, 99–07.

Hansen, B., Larsen, K.M.H., Østerhus, S., Turrell, B. and Jónsson, S., 1999. The Atlantic water inflow to the Nordic Seas. *The International WOCE Newsletter* **35**, pp. 33–35.

Hansen, B., Østerhus, S., Kristiansen, R., & Larsen, K. M. H. (1999). The Iceland–Faroe inflow of Atlantic water to the Nordic Seas. *ICES CM 1999*/L:21, 14 p.

Hansen, B., Jónsson, S., Turrell, W. R., & Østerhus, S. (2000). Seasonal variations in the Atlantic water inflow to the Nordic Seas. *ICES CM 2000*/L:03, 15 p.

Hansen, B. and Østerhus, S., 2000. North Atlantic–Nordic Seas exchanges. *Progress in Oceanography* **45**, pp. 109–208.

Hansen, B., Turrell, W.R. and Østerhus, S., 2001. Decreasing overflow from the Nordic seas into the Atlantic Ocean through the Faroe Bank channel since 1950. *Nature* **411**, pp. 927–930.

Hátún, H., Hansen, B., & Haugan, P. M. Using an "inverse dynamic method" to determine temperature and salinity fields from ADCP measurements. *Journal of Atmospheric and Oceanic Technology*, in press.

Helland-Hansen, B., & Nansen, F. (1909). The Norwegian Sea, its physical oceanography. Based on the Norwegian researches 1900–1904. *Report on Norwegian Fishery and Marine-Investigations*, *Bergen*, 2 (2).

Hermann, F., 1967. The *T–S* diagram analysis of the water masses over the Iceland–Faroe Ridge and in the Faroe Bank Channel (overflow ‘60). *Rapports et Procès-Verbaux des Réunions du Conseil International pour l’Exploration de la Mer* **157**, pp. 139–149.

Jónsson, S. and Briem, J., 2003. Flow of Atlantic water west of Iceland and onto the north Icelandic shelf. *ICES Marine Science Symposia* **219**, pp. 326–328.

Larsen, K. M. H., Hansen, B., Kristiansen, R., & Østerhus, S. (1999). *Shallow-water ADCP calibrations 1998–99*. Technical Report, The Faroese Fisheries Laboratory, 99–04.

Larsen, K.M.H., Hansen, B., Kristiansen, R. and Østerhus, S., 2000. Internal tides in the waters surrounding the Faroe Plateau. In: , p. 13.

Larsen, K. M. H., Hansen, B., & Kristiansen, R. (2000). *Nordic WOCE ADCP deployments 1999–2000*. Technical Report, The Faroese Fisheries Laboratory, 00–01.

Larsen, K. M. H., Hansen, B., & Kristiansen, R. (2001). *ADCP deployments in Faroese waters 2000–2001*. Technical Report, The Faroese Fisheries Laboratory, 01–02.

Latif, M., 2001. Tropical Pacific/Atlantic Ocean interactions at multi-decadal scales. *Geophysical Research Letters* **28** 3, pp. 539–542.

Lindau, R., 2001. In: *Climate Atlas of the Atlantic Ocean*, Springer-Verlag, Berlin, p. 514.

McCartney, M.S. and Talley, L.D., 1984. Warm-to-cold water conversion in the Northern North Atlantic Ocean. *Journal of Physical Oceanography* **14**, pp. 922–935.

Orvik, K.A., Skagseth, Ø. and Mork, M., 2001. Atlantic inflow to the Nordic Seas: current structure and volume fluxes from moored current meters, VM-ADCP and SeaSoar-CTD observations, 1995–1999. *Deep-Sea Research I* **48**, pp. 937–957.

Orvik, K.A. and Niiler, P., 2002. Major pathways of Atlantic water in the northern North Atlantic and Nordic Seas toward Arctic. *Geophysical Research Letters* **29** 19, p. 1896 (doi: 10.1029/2002GRL015002) .

Rahmstorf, S., 1999. Shifting seas in the greenhouse?. *Nature* **399**, pp. 523–524.

Read, J.F. and Pollard, R.T., 1992. Water masses in the region of the Iceland–Faeroes Front. *Journal of Physical Oceanography* **22**, pp. 1365–1378.

Roach, A.T., Aagaard, K., Pease, C.H., Salo, S.A., Weingartner, T., Pavlov, V. and Kulakov, M., 1995. Direct measurements of transport and water properties through the Bering Strait. *Journal of Geophysical Research* **100** C9, pp. 18443–18457.

Seager, R., Battisti, D.S., Yin, J., Gordon, N., Naik, N., Clement, A.C. and Cane, M.A., 2002. Is the Gulf Stream responsible for Europe’s mild winters?. *Quarterly Journal of the Royal Meteorological Society* **128**, pp. 1–24.

Simonsen, K. and Haugan, P.M., 1996. Heat budgets of the Arctic Mediterranean and sea surface heat

flux parameterizations for the Nordic Seas. *Journal of Geophysical Research* **101** C3, pp. 6553–6576.

Stefánsson, U., 1962. North Icelandic Waters. *Rit Fiskideildar* **3**, p. 269.

Turrell, W.R., Hansen, B., Hughes, S. and Østerhus, S., 2003. Hydrographic variability during the decade of the 1990s in the Northeast Atlantic and southern Norwegian Sea. *ICES Marine Science Symposia* **219**, pp. 111–120.

Valdimarsson, H. and Malmberg, S.Aa., 1999. Near-surface circulation in Icelandic waters derived from satellite tracked drifters. *Rit Fiskideildar* **16**, pp. 23–39.

Worthington, L.V., 1970. The Norwegian Sea as a Mediterranean basin. *Deep-Sea Research* **17**, pp. 77–84.

Østerhus, S. and Hansen, B., 1995. The Nordic WOCE trawl-resistant ADCP system. In: .

Østerhus, S., Turrell, W.R., Hansen, B., Lundberg, P. and Buch, E., 2001. Observed transport estimates between the North Atlantic and the Arctic Mediterranean in the Iceland–Scotland region. *Polar Research* **20** 1, pp. 169–175.

Appendix A. Error sources

A number of approximations went into the flux calculations presented. We have tested the sensitivity of the results to these by neglecting or changing the approximations and noting the effect on the calculated Atlantic water flux. Neglecting the vertical extrapolation of ADCP data (3.3 and 3.4) and assuming instead constant velocities above the uppermost good measurement gave a flux reduction of 1.5%. Current velocities were also extrapolated horizontally (Section 4.1). Neglecting the shelf velocity (instead of using 6 cm s^{-1}, as assumed) would reduce the flux by 5%. In the other end of the section, neglecting the flow through the area under station N08 was found to reduce the average Atlantic water flux by 4%.

Horizontal interpolation was used to determine velocities for each box in the flux calculation. This was done by assuming linear variation and fixed ADCP positions (Section 4.1). Varying the interpolation scheme to reflect realistic positional variation (Table 1) or non-linear interpolation gave only small flux changes, less than 2%. As previously discussed (Section 4.2), using Eqs. (4) instead of the ADCP measurements at NE and NF gave negligible changes in average flux for the 2000–2001 period and only small extra variance on shorter time scales (Fig. 19). As long as the general horizontal structure of the current (Fig. 17) remains constant, the use of these equations for the 1997–2000 period should therefore introduce only small errors. The ADCP depth is calculated from echosounding of bottom depth, corrected for sound speed variation and from mooring design. We tested the effect of errors in ADCP depth by changing the depth of the ADCP at the most critical site NB by ±20 m. The change in Atlantic water flux was about 2%.

We have tested the sensitivity of flux estimates to Eq. (7) and its salinity equivalent by assuming the temperature and salinity fields to be constant, equal to their average. The seasonal variation was, as previously noted, strongly affected, as were short-term variations, but the effect on the average Atlantic water flux was only about 2%.

In addition to the errors associated with approximations, two processes may contribute to the fluxes. Using geostrophy to extrapolate to the surface layer (Section 3.4) implies neglect of Ekman transport. From tabulated wind stress values (Lindau, 2001), the average eastward Ekman transport through the Atlantic part of section N can be estimated to approximately 0.03 Sv. This is only about 1% of the average Atlantic water flux and has a seasonal amplitude of similar magnitude.

A second process involves the loss of Atlantic water between the Iceland–Faroe Ridge and the instrumented part of section N. The fluxes in Table 4 and elsewhere have been calculated out to and including the area centered around standard station N08 (Fig. 2). This includes by far the largest part of the Atlantic water that has recently crossed the Ridge, but some of it may have been mixed out into more northerly parts of the section. Like the Ekman transport, this process would tend to increase the Atlantic water flux and the heat and salt fluxes. This water is difficult to distinguish from the Norwegian North Atlantic Water (Fig. 6), which has already recirculated in the Norwegian Basin, and it is therefore difficult to quantify. On the average, we do not think the flux of this water is likely to exceed the average flux through the area centered around station N08 (4%).

Summarizing, we find total uncertainties for the average Atlantic water flux estimate to be less than 10%, when the uncertainty in Atlantic water source characteristics is not included. For fluctuations on shorter time scales, uncertainty estimates are more difficult to perform and we will not attempt that.